MMT/Hectochelle Radial Velocity Report

8/10/2006

Chapter 1

ThAr comparison lamp - observations, data-reduction, and analysis

1.1 Goals

1. To identify "bad" lines in the ThAr linelist
2. To use high SNR ThAr exposures to determine the error/uncertainty introduced into our radial velocity measurements from the dispersion solution alone.

1.2 Data used

The ThAr and domeflat (DF) exposures used here were obtained on the nights of 11/11/2005 and 11/12/2005. Table 1.1 list relevant information for these exposures.

1.3 Data-reduction

Reduction of these data was done prior to Gabor's "hectored.sh" pipeline. Note, SM found at the time that the RMS of the dispersion solution fit (RMS of the deviations between derived and tabulated ThAr wavelengths) was different, and larger, if one trims and corrects the individual images for

Table 1.1: ThAr and DomeFlat (DF) exposures used.

Date	Type	Filename	Order	t_{exp}	Lamp mount	Fiber conf.
2005.1111	ThAr	comp.0454	RV31	900	manlifter	ring200
2005.1111	ThAr	comp.0457	RV31	900	manlifter	ring200
2005.1111	ThAr	comp.0458	RV31	900	manlifter	ring200
2005.1111	ThAr	comp.0459	RV31	900	manlifter	ring200
2005.1111	DF	domeflat.0460	RV31	2	manlifter	ring200
2005.1111	DF	domeflat.0461	RV31	1.5	manlifter	ring200
2005.1111	DF	domeflat.0462	RV31	1.5	manlifter	ring200
2005.1111	DF	domeflat.0463	RV31	1.5	manlifter	ring200
2005.1111	DF	domeflat.0464	RV31	1.5	manlifter	ring200
2005.1112	ThAr	comp.0531	RV31	600	manlifter	ring200
2005.1112	ThAr	comp.0532	RV31	600	manlifter	ring200
2005.1112	ThAr	comp.0533	RV31	600	manlifter	ring200
2005.1112	DF	domeflat.0534	RV31	2.5	manlifter	ring200

bias (CCDPROC) before combining them. In fact, when he combined the images after he CCDPROC'ed SM found the RMS of the dispersion solution from the combined ThAr was larger than the RMS of the dispersion solution for any of the individual ThAr images. SM currently has no explanation for this result and has not repeated the result recently and with the current version of the data-reduction pipeline. To test if the dependence of the RMS on the order of the CCDPROC and COMBINE persist, one could combine multiple exposures of the same type before running the reduction pipeline and compare the result to the result of a "conventional" reduction procedure.

1.3.1 Data-reduction steps for the 2005.1111 data

- CR removal
- Combine images
- CCDPROC (bias corr. + trimming)
- IMJOIN (joins 4 image sections)
- APERTURE/BACKGROUND TRACING + FLATFIELDING

- EXTRACT SPECTRA
- WAVELENGTH CALIBRATION (identify + re-identify)
- ADDING THE REFSPEC1 KEYWORD TO THE FITS HEADERS OF THE .MS FILES
- DISPERSION CORRECT THE SPECTRA

1.3.2 Data-reduction steps for the 2005.1112 data

- COMBINING IMAGES (COMP.fits)
- CCDPROC (bias corr. + trimming)
- IMJOIN (joins 4 image sections)
- COSMIC RAY REMOVAL (DF's and SF's)
- APERTURE/BACKGROUND TRACING + FLATFIELDING
- EXTRACT SPECTRA
- WAVELENGTH CALIBRATION
- ADDING THE REFSPEC1 KEYWORD TO THE FITS HEADERS OF THE .MS FILES
- DISPERSION CORRECT THE SPECTRA

1.4 Results and analysis

1.4.1 Checking for "bad" lines in the ThAr line-list

Figure 1.1 shows for the 2005.1111 combined ThAr (combined from 4 individual ThAr's) the RMS of the dispersion solution fit for all 240 (odd and even) hectochelle apertures. The RMS's span from 75 m/s to 150 m/s with a mean of 103 m/s. (Note, the standard error on the mean (SEM) shown in the figure is a calculation error.) All 56 ThAr lines from our linelist were used uncritically (sigma-clipping was turned off).

The mean RMS of the 240 dispersion solutions for each of the four individual ThAr exposures comp.0454, comp.0457, comp.0458, comp.0459 are 130, 139, 125, and 133 m/s, respectively. Thus, the expected factor of two improvement in the signal-to-noise ratio (SNR) from combining the four individual ThAr's translate into about 30 m/s lower mean RMS.

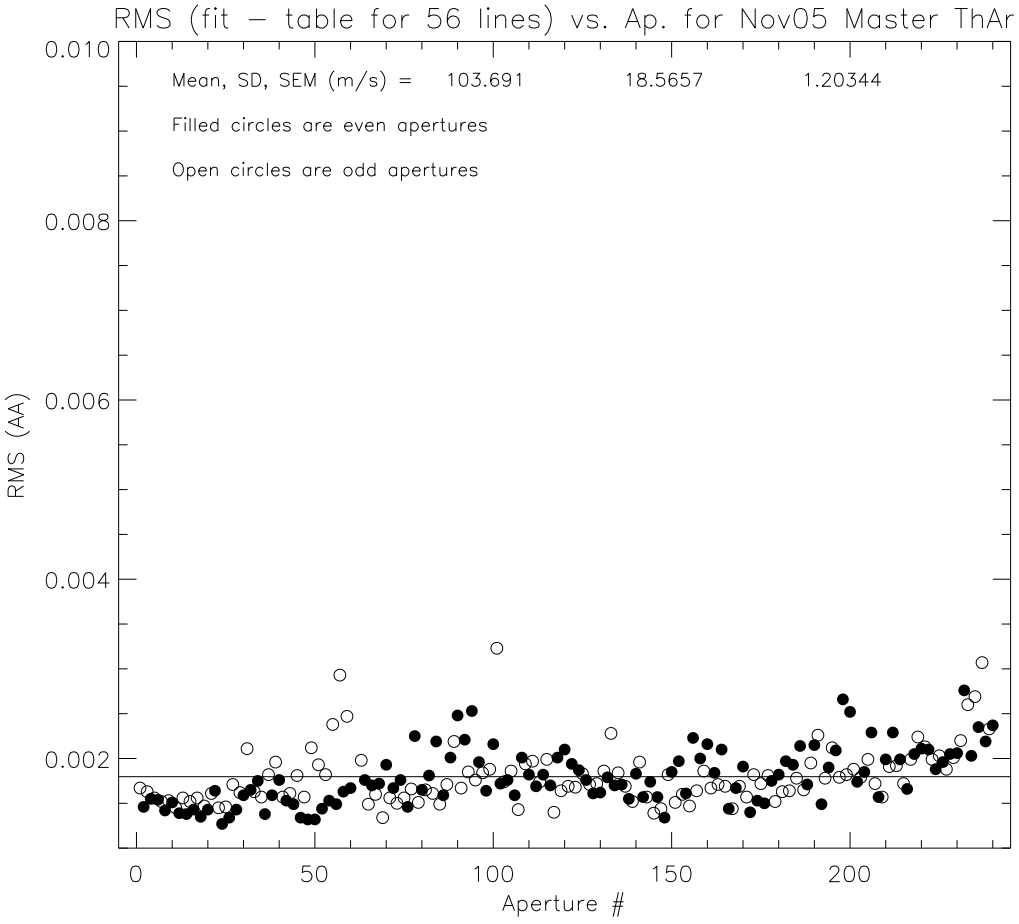

Figure 1.1: The distribution of the dispersion solution RMS of the 240 Hectochelle apertures. Each RMS represent the deviations between derived and tabulated wavelengths for all 56 ThAr lines in our linelist. Filled circles denote even aperture numbers and open circles denote odd aperture numbers.

For each ThAr there is a trend of increasing RMS with increasing aperture

number. This trend could be due to a slight tilt of the CCD chip with respect to the focal plane causing differences in the focus across the chip even though the best focus-compromise was chosen. If that is the case, then we typically focus in a way that makes the focus must be worse for higher aperture numbers.

Line 27 (5216.81396 Å) in our list of 56 ThAr lines almost always gets assigned a wavelength that deviates from the NOAO ThAr linelist value by on average 0.01 Å(or 500-600 m/s). Line 27 is almost always the most deviant of the 56 lines. Lines 45 (5273.13184 Å) and 50 (5281.62842 Å) are the 2nd and 3rd most frequent lines to have the max. deviation. We should keep an eye on those lines in the dispersion solution. Figure 1.2 shows the distribution of ThAr line numbers with the maximum deviation from the tabulated value. It clearly demonstrates the problem of assigning a wavelength to line 27.

The same is seen in the distribution of deviations for each aperture/ spectrum (Figure 1.3). Each distribution is close to "normal" and the deviation caused by line 27 falls on the far right wing of the distribution. Note, line 27 is also found to be the troublesome line from the both the 2005.1111 and the 2005.1112 ThAr data. Inspection of the ThAr spectrum gives insight into why line 27 is problematic. It is faint and "sits" on the shoulder of a brighter line.

1.4.2 Typical dispersion solution RMS and maximum ThAr line wavelength deviation

In what follows line 27 (5216.81396 Å) was removed from the ThAr linelist and sigma-clipping was turned on when determining the dispersion solution. Figure 1.4 shows the RMS vs. aperture number when determining the dispersion solution from the combined ThAr using 55 lines and sigma-clipping. The mean RMS is now 66 m/s (0.00115 Å). Determining the dispersion solution for the four ThAr individually results in mean RMS's of 78, 76, 77, and 77 m/s respectively. So the relative decrease in the mean RMS from combining four images is of order 15% or $\sim$ 10 m/s.

For the 2005.1112 ThAr exposures a similar result was found with mean RMS for each of the four individual ThAr exposures comp.0531, comp.0532, and comp.0533 of 81 m/s and a mean RMS of 69 m/s for the combined ThAr.

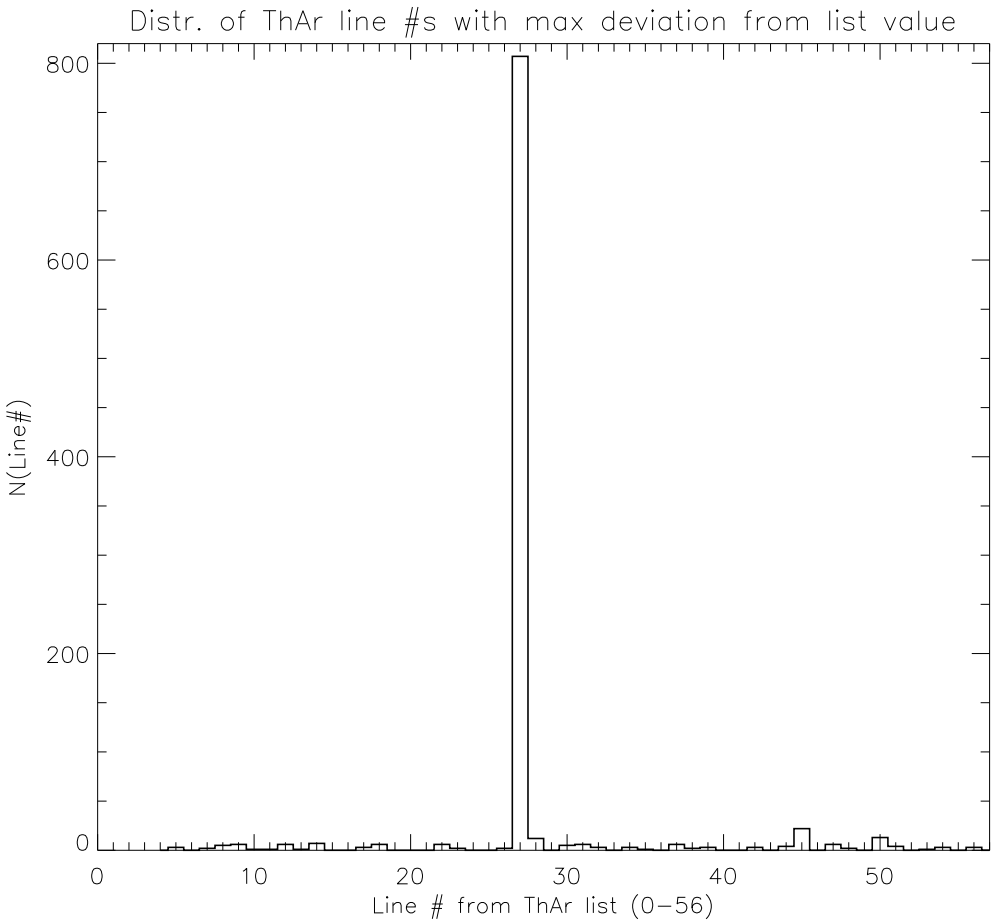

Figure 1.2: This histogram shows the frequency with which each of the 56 ThAr lines was found to be the most deviant from the tabulated ThAr line wavelength. Line 27 in our linelist (5216.81396 Å) stand out as a consistent problematic line.

Figure 1.5 shows the distribution of ThAr line numbers with the maximum deviation from the tabulated value. It appears that three lines are most frequently the ones with the max deviations. Those lines are 17 (5258.3602 Å), 35 (5199.1637 Å), and 55 (5151.612 Å). However, the max. deviations are of the order 150-200 m/s compared to $\sim$ 500-600 m/s for line 27.

Figure 1.6 shows the distribution of the maximum deviations resulting

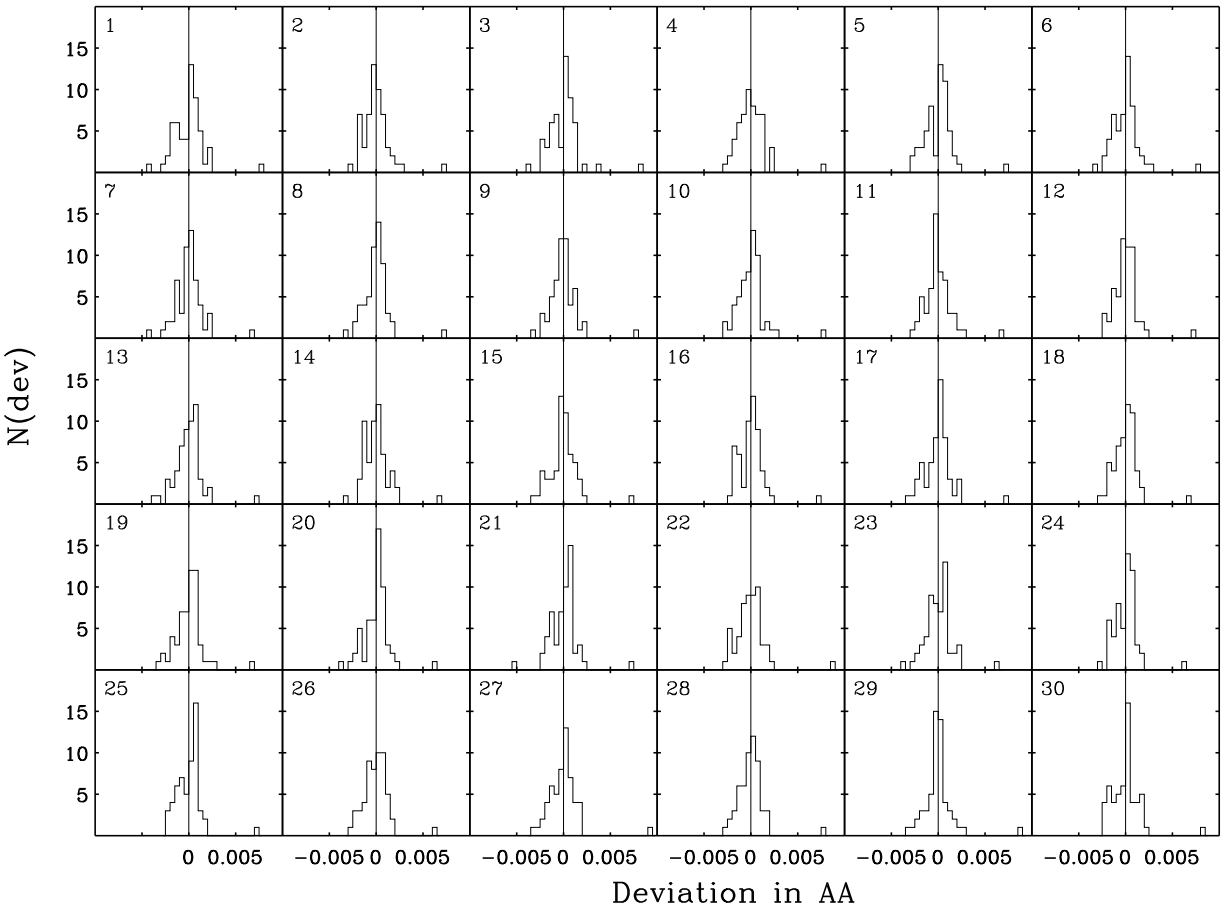

Figure 1.3: The distributions of the 56 wavelength deviations for the first 30 Hectochelle apertures. The obvious outlier on the far right wing of the distribution is line 27 (5216.81396 Å).

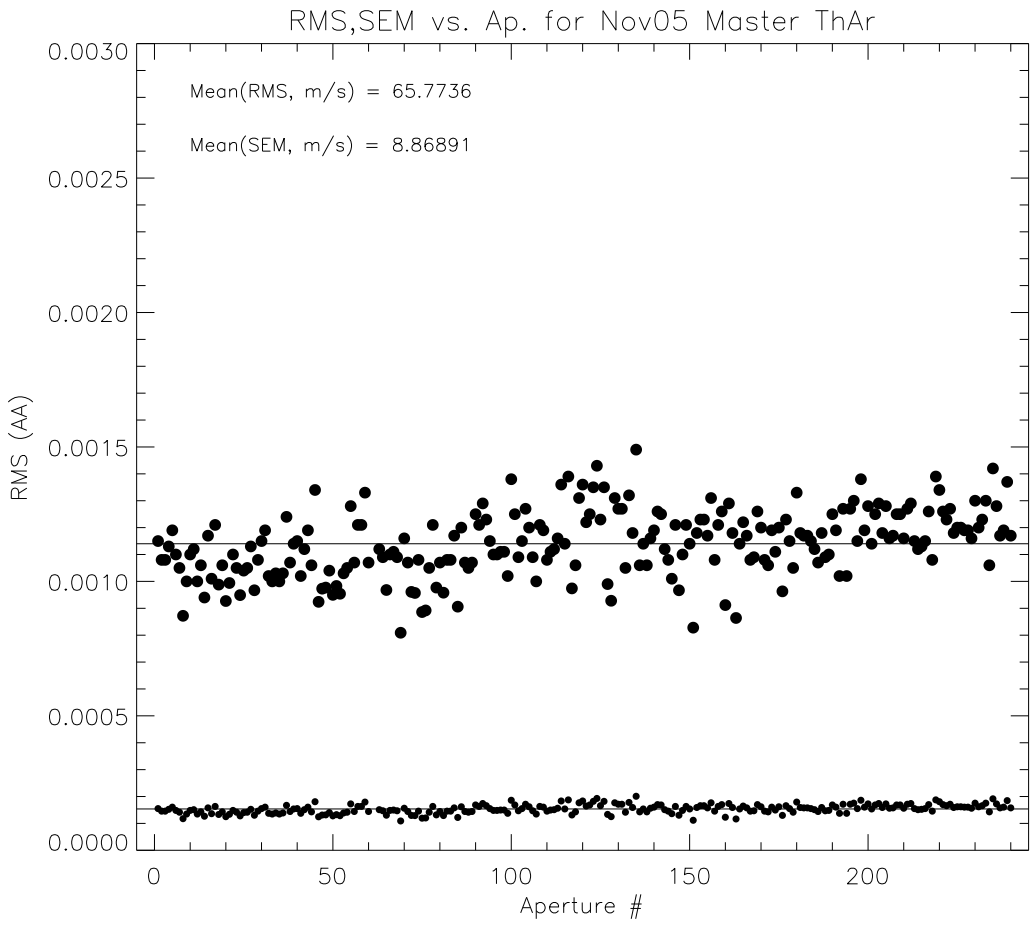

Figure 1.4: The RMS vs. aperture when determining the dispersion solution from the combined ThAr from 2005.1111 and excluding line 27 from the ThAr linelist. The mean RMS is now 66 m/s (0.00115 Å).

from the 240 solutions from all 5 ThAr's. The mode of the distribution is about 0.003 Åwhich corresponds to $\sim$ 170 m/s. In Figure 1.7 these same max. deviations are shown as a function of the aperture number. There is a slight trend toward on average larger max. deviations for larger aperture number, similar behaviour as the RMS.

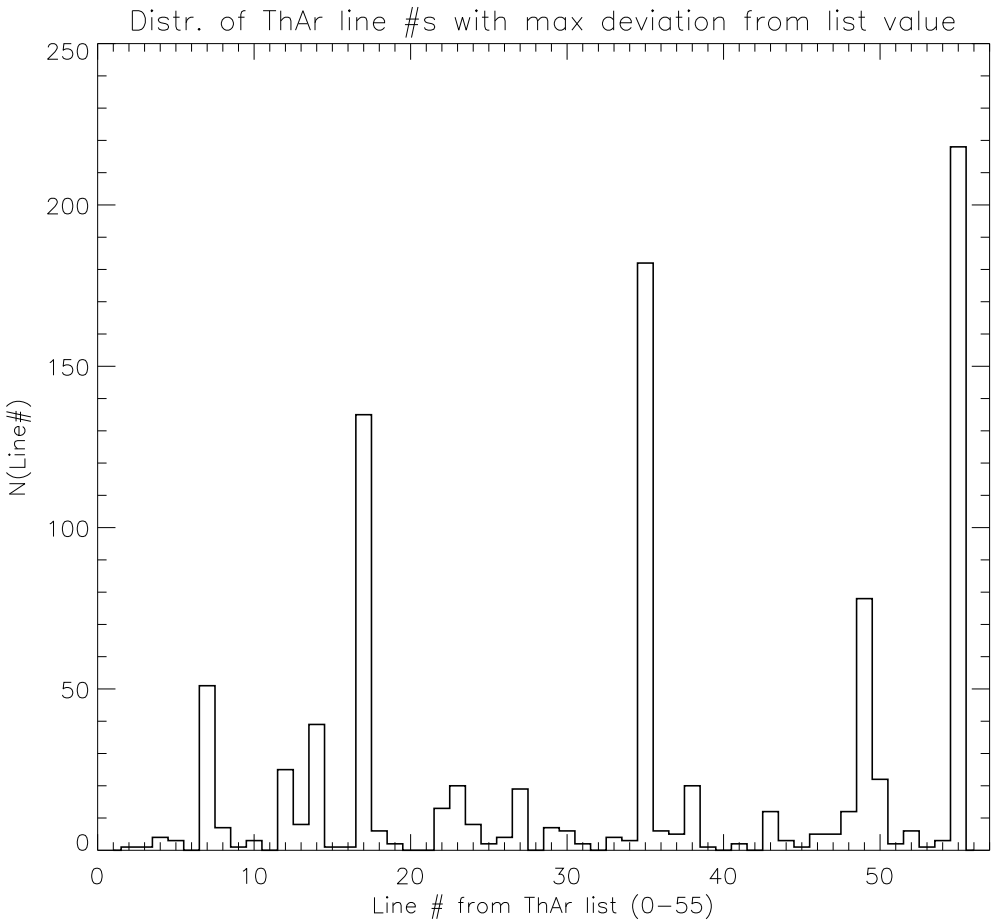

Figure 1.5: The distribution of ThAr line numbers with the maximum deviation from the tabulated value. Lines 17 (5258.3602 Å) 35 (5199.1637 Å), and 55 (5151.612 Å) most frequently have the maximum deviations.

1.4.3 Time-stability of the dispersion solution and velocity shifts between adjacent ThAr exposures

As a study of the stability of the dispersion solution we show in Figure 1.8 the RMS from the combined 2005.1111 ThAr as black dots and the interval between the minimum and maximum RMS' from the four individual 2005.1111 ThAr's as grey vertical lines. The difference between the max. and min.

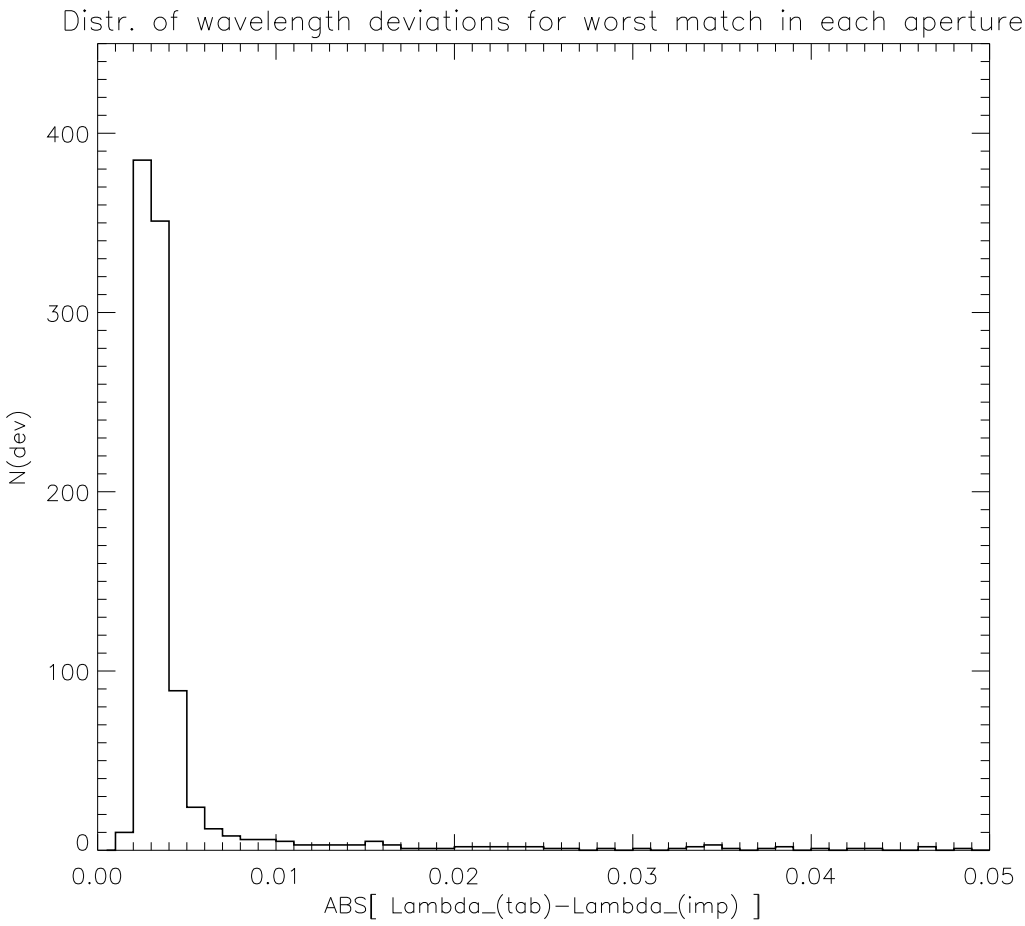

Figure 1.6: A histograms of the 1200 maximum deviations from 240 apertures in 5 ThAr exposures from 2005.1111 and 2005.1112. **DL:** shouldn't sigma-clipping prevent the tail toward largest deviations? **SM:** Have to check to absolutely sure the histogram is for sigma-clipping turned on. I am pretty sure it is and that the larger max. deviations are from the occasional poor dispersion solution with inflated deviations for all lines.

RMS for any given aperture is $\sim$ 0.0003 Åwhich corresponds to $\sim$ 20-30 m/s. Also shown in Figure 1.8 is the standard error on the mean (SEM = RMS/sqrt(55)) for from the combined 2005.1111 ThAr. The typical SEM is $\sim$ 0.00016 Åwhich corresponds to $\sim$ 10 m/s. Considering the normal distribu-

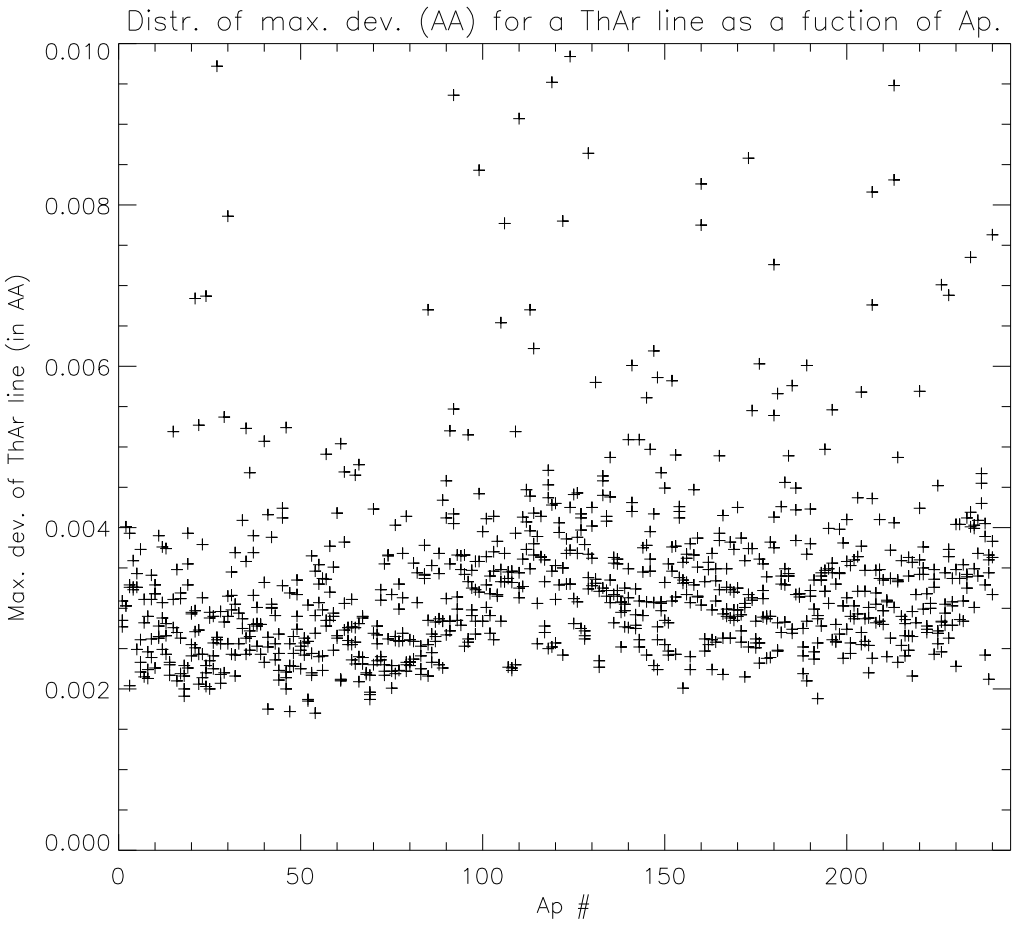

Figure 1.7: The maximum deviations shown as a fct of aperture number. A slight increase in the max. deviation with increasing aperture number follows the trend of increased dispersion solution RMS with increasing aperture number. The reason is presumably the same and presumably a gradient in the image focus.

tion of the wavelength deviations seen in Figure 1.3, it is perhaps reasonable to estimate the actual uncertainty on the dispersion solution as the SEM of the 55 individual deviations. Of course, our real interest is to estimate at what level the dispersion solution contributes to the overall radial-velocity uncertainty. One way to test this empirically is to calculate the relative

shifts between two dispersion corrected ThAr spectra. Figure 1.9 shows the velocity shifts (in km/s) between the corresponding 240 ThAr spectra from the 2005.1111 ThAr exposures comp.0457 and comp.0458. The mean of this distribution represents the degree of a systematic shift, while the scatter around 0 is a measure of the uncertainty in the dispersion solution. The RMS scatter for the case shown in Figure 1.9 is $\sim$ 18.5 m/s. From several similar experiments with cross-correlation of corresponding ThAr spectra in the 2005.1111 and 2005.1112 ThAr exposures, we find that the RMS of the relative velocity shifts are of the order 15-30 m/s, similar to the SEM's of the dispersion solutions. We conclude from here that the precision-limit being put on the radial velocity precision work with MMT/Hectochelle is set by the ThAr dispersion solution at $\sim$ 20-30 m/s.

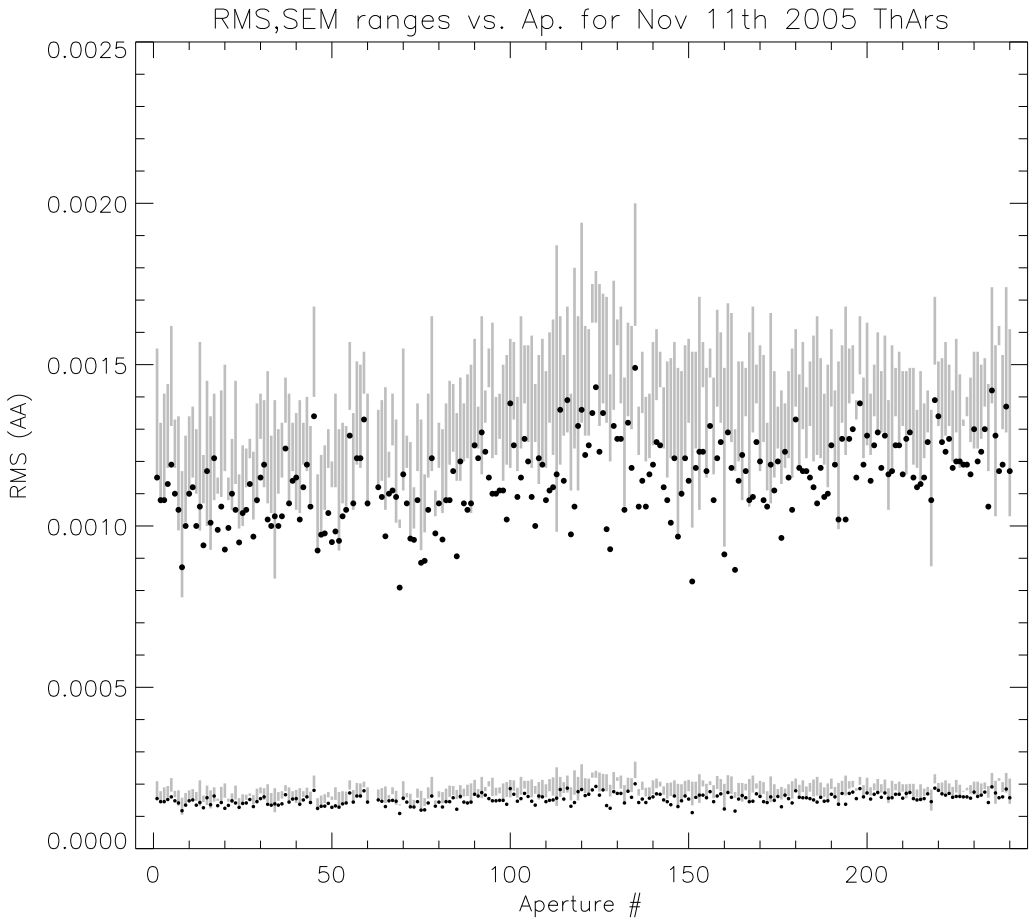

Figure 1.8: The RMS distribution with aperture number for the combined 2005.1111 ThAr (black dots), and the interval between the minimum and maximum RMS (vertical grey lines) for each aperture and for four individual 2005.1111 ThAr exposures. The difference between the max. and min. RMS for any given aperture is $\sim$ 0.0003 Åwhich corresponds to $\sim$ 20-30 m/s. Also shown is the standard error on the mean (SEM = RMS/sqrt(55)). The typical SEM is $\sim$ 0.00016 Åwhich corresponds to $\sim$ 10 m/s.

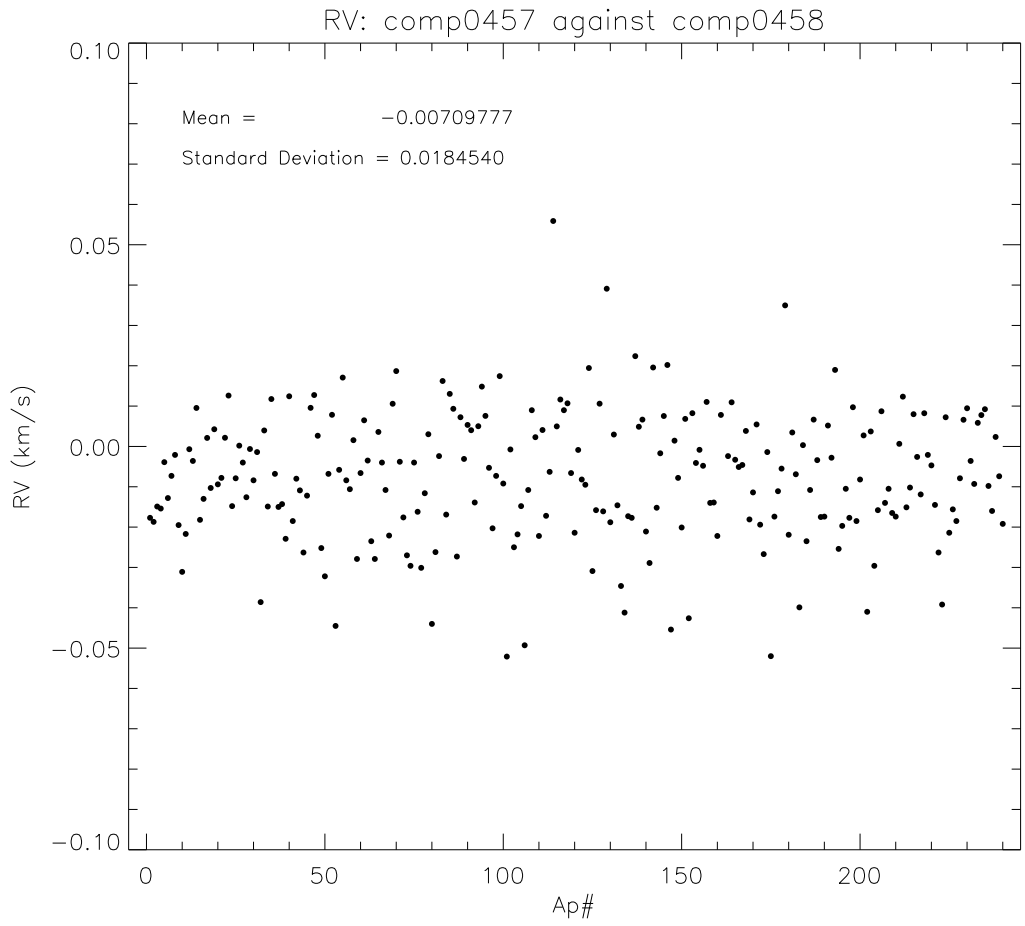

Figure 1.9: The the velocity shifts (in km/s) between the corresponding 240 ThAr spectra from the 2005.1111 ThAr exposures comp.0457 and comp.0458. The RMS scatter of the velocity shifts is $\sim$ 18.5 m/s.

Chapter 2

Sky-exposures - observations, data-reduction, and analysis

2.1 Goals

1. To determine fiber-to-fiber radial-velocity variations in Hectochelle and, if systematic, provide corrections for such variations.

2. To determine night-to-night (run-to-run) radial-velocity variations in Hectochelle and, if systematic, provide corrections for such variations.

3. To correct for potential systematic (fiber-to-fiber and run-to-run) to determine the *upper limit* on the Hectochelle radial-velocity measurement precision and accuracy from the repeatability and values of the Sun's velocity derived from sky-exposures.

2.2 Approach

In Hectochelle the radial velocities derived from each of the 240 fibers differs. Fiber-to-fiber variations of the order 500 m/s is observed when measuring the velocity of the Sun from sky-exposures. If these velocity differences between fibers are not varying with time - if they are stable, then they can be measured and corrected for.

The approach to measuring fiber-to-fiber variations is the following. A measurement of the radial velocity of the Sun with respect to us should, when corrected for the relative velocity between the solar disk and the part of the

earths atmosphere at which we are looking (correction for rate of change of distance between Sun and earth at the time of the observation, correction for earth's rotation, and correction for gravitational redshift of the solar radiation), result in a value within the intrinsic measurement uncertainty from zero. If repeated measurements of the solar radial velocity through the same fiber are distributed evenly around zero, then the deviations are due to the random measurement uncertainties of the instrument. If however, the measurements from the same fiber fall systematically above or below zero, then this offset can be determined through repeated measurements and corrected for. However, due to instabilities of the spectrograph and numerous unknown factors there may also be a systematic offset from zero of the velocities from all fibers. This general offset may change from night to night and from run to run. Our best estimate of such a general offset will be the mean velocity over all fibers for a given afternoon. The general offset can be referred to as a night-to-night (or run-to-run) variation. Because of such potential night-to-night variations the deviation of any individual velocity from a given fiber must be measured not from zero but from the mean of all 240 velocities. This step will eliminate the contribution of the night-to-night velocity variations, and leave a relative deviation - from the mean.

2.3 Data used

To determine fiber-to-fiber variations in the Hectochelle spectrograph we have derived radial velocities from sky-exposures from 12 different afternoons spanning in time from October 21st 2005 to May 10th 2006 (2005.1021, 2005.1112, 2005.1114, 2005.1115, 2006.0316, 2006.0406, 2006.0407, 2006.0421, 2006.0424, 2006.0425, 2006.0508, and 2006.0510). On each of the 12 afternoons high signal-to-noise sky-exposures were obtained through all 240 fibers. Table 2.1 list all sky, domeflat, and comparison (ThAr) exposures used for this study. If more than one exposure of a specific type were obtained, the multiple exposures were combined as part of the data reduction.

Table 2.1: Sky-, domeflat-, and ThAr-exposures from 12 afternoons from October 2005 to May 2006.

Date	Type	Filename	Order	t_{exp}	Lamp mount	Fiber conf.
2005.1021	ThAr	comp.0367	RV31	180	manlifter	ring250
2005.1021	ThAr	comp.0368	RV31	600	manlifter	ring250
2005.1021	ThAr	comp.0369	RV31	300	manlifter	ring250
2005.1021	DF	domeflat.0370	RV31	1.2	manlifter	ring250
2005.1021	DF	domeflat.0371	RV31	1.2	manlifter	ring250
2005.1021	DF	domeflat.0372	RV31	1.2	manlifter	ring250
2005.1021	DF	domeflat.0373	RV31	1.2	manlifter	ring250
2005.1021	DF	domeflat.0374	RV31	1.2	manlifter	ring250
2005.1021	SF	sflat.0375	RV31	10	manlifter	ring250
2005.1021	SF	sflat.0376	RV31	5	manlifter	ring250
2005.1021	SF	sflat.0377	RV31	5	manlifter	ring250
2005.1021	SF	sflat.0378	RV31	10	manlifter	ring250
2005.1021	SF	sflat.0379	RV31	10	manlifter	ring250
2005.1112	ThAr	comp.0531	RV31	600	manlifter	ring200
2005.1112	ThAr	comp.0532	RV31	600	manlifter	ring200
2005.1112	ThAr	comp.0533	RV31	600	manlifter	ring200
2005.1112	ThAr	comp.0549	RV31	1800	manlifter	ring200
2005.1112	ThAr	comp.0550	RV31	1800	manlifter	ring200
2005.1112	DF	domeflat.0534	RV31	2.5	manlifter	ring200
2005.1112	SF	sflat.0536	RV31	20	manlifter	ring200
2005.1112	SF	sflat.0537	RV31	35	manlifter	ring200
2005.1112	SF	sflat.0538	RV31	50	manlifter	ring200
2005.1112	SF	sflat.0539	RV31	60	manlifter	ring200
2005.1112	SF	sflat.0540	RV31	75	manlifter	ring200
2005.1112	SF	sflat.0541	RV31	100	manlifter	ring200
2005.1114	ThAr	comp.0703	RV31	300	manlifter	ring200
2005.1114	DF	domeflat.0704	RV31	1.0	manlifter	ring200
2005.1114	SF	sflat.0687	RV31	30	manlifter	ring200
2005.1114	SF	sflat.0688	RV31	10	manlifter	ring200
2005.1115	ThAr	comp.0800	RV31	600	manlifter	ring200
2005.1115	ThAr	comp.0819	RV31	900	manlifter	ring200

Continued on next page...

Table 2.1 – continued from previous page

Date	Type	Filename	Order	t_{exp}	Lamp mount	Fiber conf.
2005.1115	DF	domeflat.0793	RV31	1.0	manlifter	ring200
2005.1115	DF	domeflat.0794	RV31	1.0	manlifter	ring200
2005.1115	DF	domeflat.0795	RV31	1.0	manlifter	ring200
2005.1115	SF	sflat.0801	RV31	1	manlifter	ring200
2005.1115	SF	sflat.0802	RV31	10	manlifter	ring200
2005.1115	SF	sflat.0803	RV31	15	manlifter	ring200
2005.1115	SF	sflat.0804	RV31	20	manlifter	ring200
2005.1115	SF	sflat.0805	RV31	60	manlifter	ring200
2005.1115	SF	sflat.0806	RV31	75	manlifter	ring200
2005.1115	SF	sflat.0807	RV31	90	manlifter	ring200
2005.1115	SF	sflat.0808	RV31	110	manlifter	ring200
2005.1115	SF	sflat.0809	RV31	130	manlifter	ring200
2006.0316	ThAr	comp.0702	RV31	900	secondary	ring250
2006.0316	DF	domeflat.684	RV31	24	secondary	ring250
2006.0316	DF	domeflat.685	RV31	24	secondary	ring250
2006.0316	DF	domeflat.686	RV31	24	secondary	ring250
2006.0316	SF	sflat.0706	RV31	10	secondary	ring250
2006.0316	SF	sflat.0707	RV31	10	secondary	ring250
2006.0406	ThAr	comp.0948	RV31	1800	secondary	ring250
2006.0406	ThAr	comp.0949	RV31	1800	secondary	ring250
2006.0406	ThAr	comp.0950	RV31	1800	secondary	ring250
2006.0406	DF	domeflat.0945	RV31	40	secondary	ring250
2006.0406	DF	domeflat.0946	RV31	40	secondary	ring250
2006.0406	DF	domeflat.0947	RV31	50	secondary	ring250
2006.0406	SF	sflat.0960	RV31	25	secondary	ring250
2006.0406	SF	sflat.0961	RV31	40	secondary	ring250
2006.0406	SF	sflat.0962	RV31	60	secondary	ring250
2006.0407	ThAr	comp.1037	RV31	1800	secondary	ring250
2006.0407	ThAr	comp.1038	RV31	1800	secondary	ring250
2006.0407	ThAr	comp.1039	RV31	1800	secondary	ring250
2006.0407	DF	domeflat.1040	RV31	40	secondary	ring250
2006.0407	DF	domeflat.1041	RV31	40	secondary	ring250

Continued on next page...

Table 2.1 – continued from previous page

Date	Type	Filename	Order	t_{exp}	Lamp mount	Fiber conf.
2006.0407	DF	domeflat.1042	RV31	40	secondary	ring250
2006.0407	SF	sflat.1060	RV31	40	secondary	ring250
2006.0407	SF	sflat.1061	RV31	55	secondary	ring250
2006.0407	SF	sflat.1062	RV31	80	secondary	ring250
2006.0421	ThAr	comp.1354	RV31	900	secondary	ring250
2006.0421	DF	domeflat.1344	RV31	24	secondary	ring250
2006.0421	DF	domeflat.1345	RV31	24	secondary	ring250
2006.0421	DF	domeflat.1346	RV31	24	secondary	ring250
2006.0421	DF	domeflat.1347	RV31	24	secondary	ring250
2006.0421	DF	domeflat.1348	RV31	24	secondary	ring250
2006.0421	SF	sflat.1359	RV31	30	secondary	ring250
2006.0421	SF	sflat.1360	RV31	45	secondary	ring250
2006.0421	SF	sflat.1361	RV31	60	secondary	ring250
2006.0424	ThAr	comp.1414	RV31	900	secondary	ring250
2006.0424	DF	domeflat.1404	RV31	24	secondary	ring250
2006.0424	DF	domeflat.1405	RV31	24	secondary	ring250
2006.0424	DF	domeflat.1406	RV31	24	secondary	ring250
2006.0424	DF	domeflat.1407	RV31	24	secondary	ring250
2006.0424	DF	domeflat.1408	RV31	24	secondary	ring250
2006.0424	SF	sflat.1417	RV31	60	secondary	ring250
2006.0424	SF	sflat.1418	RV31	60	secondary	ring250
2006.0424	SF	sflat.1419	RV31	70	secondary	ring250
2006.0425	ThAr	comp.1521	RV31	1200	secondary	ring275
2006.0425	ThAr	comp.1522	RV31	1200	secondary	ring275
2006.0425	ThAr	comp.1523	RV31	1200	secondary	ring275
2006.0425	DF	domeflat.1524	RV31	24	secondary	ring275
2006.0425	DF	domeflat.1525	RV31	24	secondary	ring275
2006.0425	DF	domeflat.1526	RV31	24	secondary	ring275
2006.0425	DF	domeflat.1527	RV31	24	secondary	ring275
2006.0425	DF	domeflat.1528	RV31	24	secondary	ring275
2006.0425	SF	sflat.1534	RV31	45	secondary	ring275
2006.0425	SF	sflat.1535	RV31	60	secondary	ring275

Continued on next page...

Table 2.1 – continued from previous page

Date	Type	Filename	Order	t_{exp}	Lamp mount	Fiber conf.
2006.0425	SF	sflat.1536	RV31	75	secondary	ring275
2006.0425	SF	sflat.1537	RV31	120	secondary	ring275
2006.0508	ThAr	comp.1670	RV31	900	secondary	ring250
2006.0508	ThAr	comp.1694	RV31	240	secondary	ring250
2006.0508	ThAr	comp.1701	RV31	240	secondary	ring250
2006.0508	DF	domeflat.1671	RV31	24	secondary	ring250
2006.0508	DF	domeflat.1672	RV31	24	secondary	ring250
2006.0508	DF	domeflat.1673	RV31	24	secondary	ring250
2006.0508	DF	domeflat.1674	RV31	24	secondary	ring250
2006.0508	DF	domeflat.1675	RV31	24	secondary	ring250
2006.0508	DF	domeflat.1676	RV31	24	secondary	ring250
2006.0508	DF	domeflat.1677	RV31	24	secondary	ring250
2006.0508	DF	domeflat.1678	RV31	24	secondary	ring250
2006.0508	DF	domeflat.1679	RV31	24	secondary	ring250
2006.0508	DF	domeflat.1680	RV31	24	secondary	ring250
2006.0508	SF	sflat.1696	RV31	12	secondary	ring250
2006.0508	SF	sflat.1697	RV31	12	secondary	ring250
2006.0508	SF	sflat.1698	RV31	12	secondary	ring250
2006.0508	SF	sflat.1699	RV31	12	secondary	ring250
2006.0508	SF	sflat.1700	RV31	12	secondary	ring250
2006.0510	ThAr	comp.1938	RV31	240	secondary	ring250
2006.0510	ThAr	comp.1946	RV31	240	secondary	ring250
2006.0510	DF	domeflat.1902	RV31	24	secondary	ring250
2006.0510	DF	domeflat.1903	RV31	24	secondary	ring250
2006.0510	DF	domeflat.1904	RV31	24	secondary	ring250
2006.0510	DF	domeflat.1905	RV31	24	secondary	ring250
2006.0510	DF	domeflat.1906	RV31	24	secondary	ring250
2006.0510	DF	domeflat.1907	RV31	24	secondary	ring250
2006.0510	DF	domeflat.1908	RV31	24	secondary	ring250
2006.0510	DF	domeflat.1909	RV31	24	secondary	ring250
2006.0510	SF	sflat.1940	RV31	15	secondary	ring250
2006.0510	SF	sflat.1941	RV31	15	secondary	ring250

Continued on next page...

Table 2.1 – continued from previous page

Date	Type	Filename	Order	t_{exp}	Lamp mount	Fiber conf.
2006.0510	SF	sflat.1942	RV31	15	secondary	ring250
2006.0510	SF	sflat.1943	RV31	15	secondary	ring250
2006.0510	SF	sflat.1944	RV31	15	secondary	ring250

2.4 Data-reduction

Reduction of the data from all 12 afternoons was done in a consistent manner following the Hectochelle reduction pipeline developed by Gabor (hectored.sh). Below follows a brief description of the steps involved from raw images to extracted and corrected one-dimensional spectra:

1. Basic image processing:
    - Bias subtraction using a 11th order spline3 fit to the overscan region (biassec=[1080:1120,3:4603]) and 3σ high/low clipping.
    - Trimming the CCD image using trimsec=[51:1074,3:4603].
    - Joining the four image sections (one per amplifier) into one image and adding the GAIN (1.0), RDNOISE (2.7), IMJOIN, and HP_STP3 keywords to the image header of the combined image.
    - Cosmic ray removal through median filtering over a 5 column x 13 line box using a threshold of 3σ.
    - Combining multiple exposures of the same target using the median as the estimate for the true intensity after rejection of "bad" pixels with CCDCLIP. SM has found that the RMS of the dispersion solution fit is larger if one trim and correct the individual images for bias (CCDPROC) before combining them.
    - Combine flatfields (domeflats) if more than one (median, no rejection).
    - Combine comparison exposures (ThAr) if more than one (median, no rejection).

- Determine if cosmic ray removal was done ... *** ONLY DONE IF MORE THAN ONE IMAGE ...?? Checks if OBJECT_cr.fits exist ? ***
- Finding and tracing the apertures in the domeflat image (IRAF apall) using a spline3 (cubic spline) tracing function of 5th order (5 spline pieces). Determine offset between the X pixel-coordinate of aperture 120 in the actual image and the X pixel-coordinate of the aperture 120 as taken from a general aperture reference file (located in the MASTER_DATABASE directory). Applying this offset to the "center" coordinate of all apertures in the reference file and writing it to the IRAF database directory. Note, this step is necessary because of shifts caused by temperature variations in the spectrograph room.
- Re-center aperture positions in cross-dispersion direction (IRAF aprecenter). Updated aperture reference file created in "database" directory.
- The updated aperture reference file is given as input to to IRAF aprecenter task and the position of the spectrum is traced (IRAF aptrace) within each domeflat aperture and a 5th order cubic spline (spline3) is fit to the trace.
- IRAF apflat is used to create an APFLAT image used to correct for pixel-to-pixel variations by division (divide OBJECT, COMP, and DOME with APFLAT image). **SM:** Why don't we extract before we flatfield? **DL:** Because illumination pattern is non-uniform and may shift with time.

2. Recenter (IRAF aprecenter) the aperture trace positions for the domeflat, ThAr, and object exposures ... *** ? ***

3. Extract the flux in apertures into one dimensional spectra (IRAF apall). No background subtraction is used. *** pfit=fit1d ? ***

4. Update REFSPEC header keyword in domeflat, ThAr, object multispec files.

5. Dispersion correction (pixel-to-wavelength mapping). A "master" dispersion solution is initially used as a first guess for the dispersion solution. By re-fitting, this initial solution is used to determined wave-

lengths for the 55 ThAr lines. Sigma-clipping of "bad" lines is done based on the deviations from the nominal wavelengths in the NOAO/IRAF linelist, and so the final solution is based on a best fit to the remaining pixel-wavelength points. There are known issues with this important step. IRAF occasionally detects a number of non-lines causing the total number of lines to exceed 55. These erroneous line-detections may be caused by noise, cosmic events, etc., but importantly are not necessarily removed in the sigma-clipping process. An attempt to solve this problem is under way ...

6. Normalizing fiber throughputs ...

7. Skysubtraction ... (Not currently part of the pipeline!)

8. Continuum normalization ...

2.5 Results and analysis

2.5.1 Fiber-to-fiber radial-velocity variations

By cross-correlation (IRAF xcsao) of a combined sky-exposure with a synthetic template the radial velocity of the Sun was determined for each fiber for each afternoon. The synthetic template (t05750g45p00ap00k2v002z1i85) was chosen as close to solar as possible: Teff = 5750, log(g) = 4.5, [Fe/H] = 0, vsin(i) = 2 km/s, and with an instrumental profile similar to Hectochelle spectra (**SM:** Needs further investigation.). Correction for relative motion within the solar system was done using the IRAF task BCVCORR (by Doug Mink). The velocity corrections applied here are a relative velocity between the geocenter and heliocenter, the rotational velocity of the observatory on the earth's surface relative to the Sun, and a correction for the gravitational redshift of the solar radiation (we apply a correction of -636 m/s).

We show in Figure 2.1 the radial-velocities of the sun for all 240 fibers determined from the combined sky-exposure from 2006.0407. We note the systematic offset from zero that decreases for the highest aperture numbers as well as the fiber-to-fiber variations of the order of 500 m/s.

In summary, we have for each of the 240 hectochelle fibers 12 radial velocities of the Sun from 12 different afternoons. In Figure 2.2 we show the

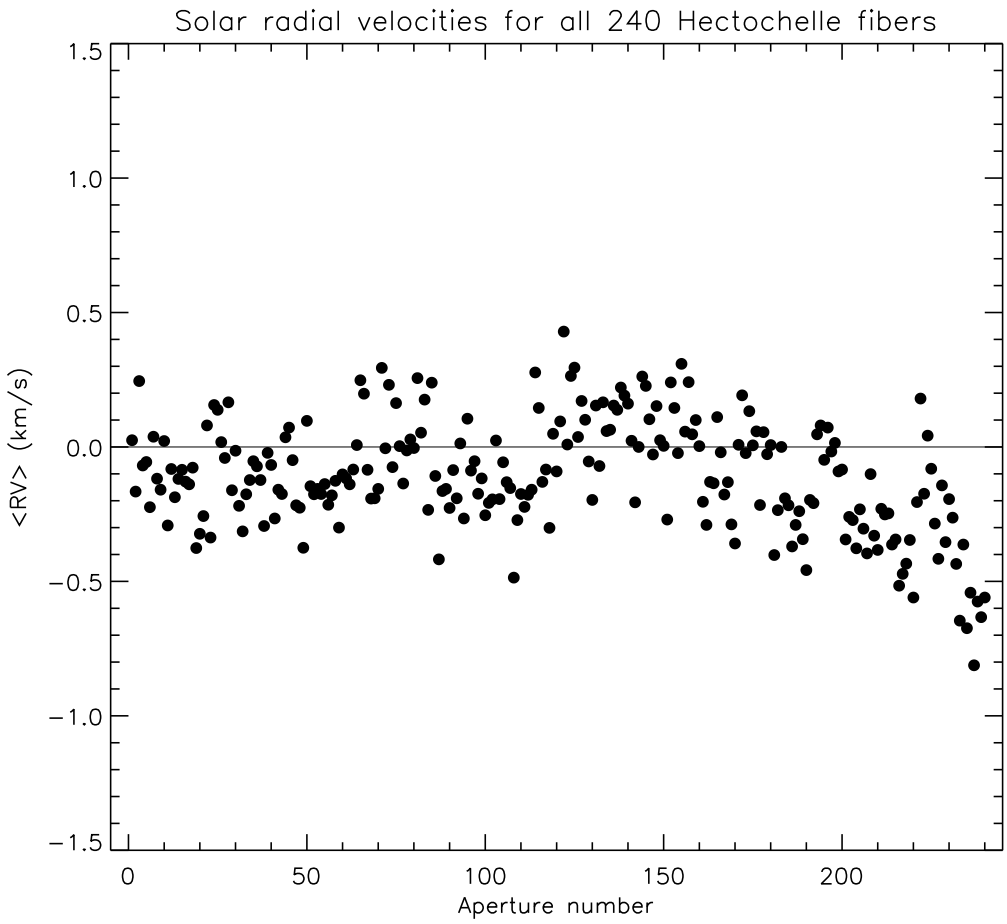

Figure 2.1: Radial-velocities of the sun for all 240 fibers determined from the combined sky-exposure from 2006.0407. Velocities are corrected for a relative velocity between the geocenter and heliocenter, the rotational velocity of the observatory on the earth's surface relative to the Sun, and a correction for the gravitational redshift of the solar radiation (-636 m/s).

mean of the 240 solar velocities for each of the 12 afternoons. The errorbars represent the standard deviation of the 240 velocities.

The grouping in time in Figure 2.2 correspond to data from the October/November (fall) 2005 and from April/May (spring) 2006. The horizontal dashed lines show the mean values of the fall and spring offsets. Each

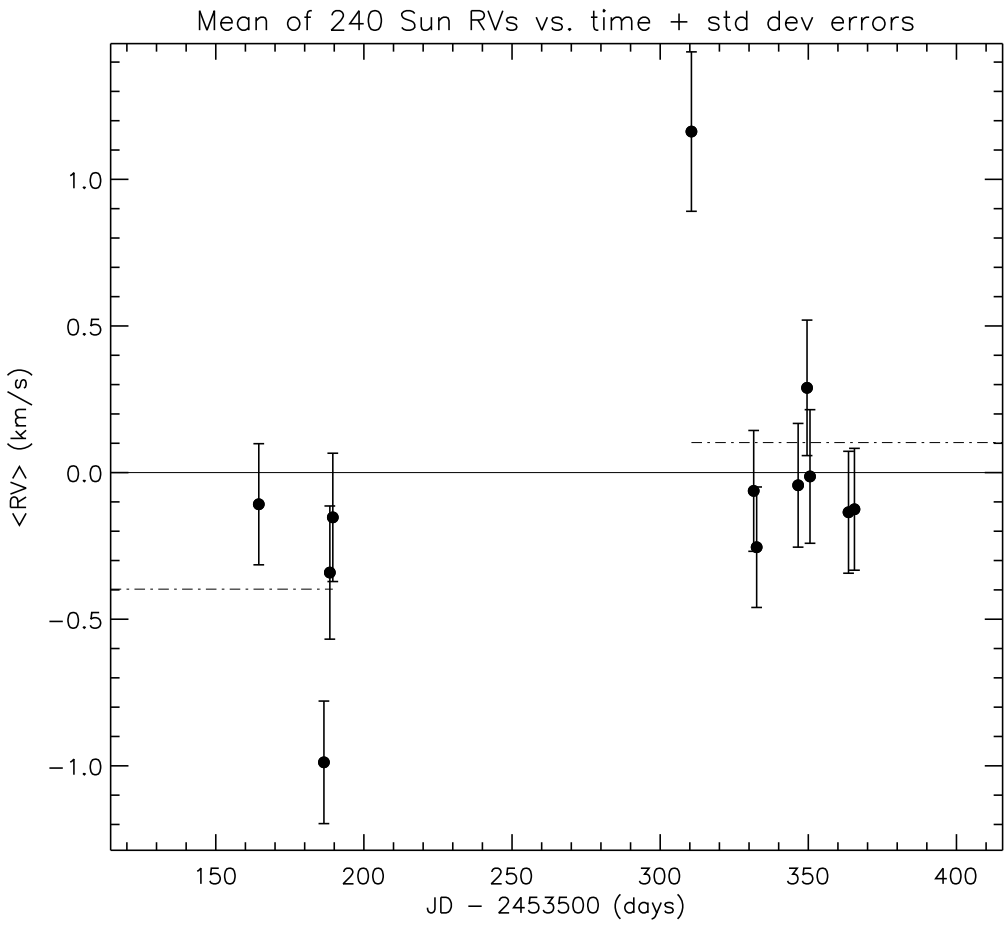

Figure 2.2: The means of all 240 solar velocities for each of the 12 afternoons. The errorbars represent the standard deviation of the 240 velocities and the horizontal dashed lines shows the means of the fall 2005 means (JD-2453500 $<$ 200 days) and the spring 2006 means (JD-2453500 $>$ 300 days).

group/sample of means has a deviating point (2005.1112 and 2006.0316). The 2006.0316 dispersion solution, based on one 900 second ThAr, resulted in abnormally high RMS's for intermediate aperture numbers. We show in Figure 2.3 the distribution of RMS vs. aperture number for the dispersion solution from 2006.0316 and in Figure 2.4 a more typical result from 2006.0406. Note also that the 2006.0316 sky-exposures were fewer (2) and shorter (10

sec) than those from other nights (see Table 2.1). Consequently, for the time being, less weight should be put on the deviant mean for the afternoon of 2006.0316 in Figure 2.2. The other deviant mean in Figure 2.2 is from 2005.1112. There is no clear indication of a poor dispersion solution and a total of 5 long ThAr are used. We recall that the offsets from 0 km/s of the means in Figure 2.2 are not due to relative motions within the solar system as we have corrected for those as explained above.

In general, with the exceptions of the means from 2005.1112 and 2006.0316, the mean velocity over the 240 fibers falls consistently within 1-2 standard deviations from zero. When excluding the 2005.1112 and 2006.0316 means, there may be a slight systematic offset between the fall 2005 sample (*calibration lamps mounted on manlifter*) and the spring 2006 sample (*calibration lamps mounted permanently on secondary*). Overall this is a good indication that the spectrograph is well behaved.

We proceed to use the mean velocities shown in Figure 2.2 as reference velocities to calculate fiber-to-fiber variations. For each night we calculate the deviations between the mean velocities and the velocities of the 240 individual fibers. The result is 12 deviations for each fiber. Figure 2.5 shows for aperture numbers 41-60 the 12 deviations vs. time (MJD - 2453500). Similar plots for all apertures can be found in Apppendix A. As can be seen for these 20 apertures, most often the velocity from a given fiber is consistently above or below zero. However, frequently a systematic difference between the fall 2005 deviations and the spring 2006 deviations is visible, and the deviations from the afternoons of 2005.1112 and 2006.0316 deviates from the other 10. More so than for the fall 2005 velocities, the deviations of the more recent spring 2006 velocities for a given fiber are consistently positive, negative, or close to zero, which is critical to our ability to correct for these deviations. In Appendix A Figure A.13 we also show the difference between the mean of the deviations from fall 2005 and from spring 2006. The symmetric scatter around zero in Figure A.13 indicate that there is no systematic difference/offset between the deviations before and after the permanent mount of the calibrations lamps. Figure A.14, however, shows that the standard deviation of the fall 2005 deviations are typically larger than the standard deviations of the spring 2006 deviations.

We show in Figure 2.6 the mean of the 12 deviations for each of the 240 fibers (represented on the abscissa by their aperture numbers). Note that aperture numbers do not equal fiber numbers (see Figure **??** in Appendix A). The errorbars represent the standard deviation of the 12 deviations.

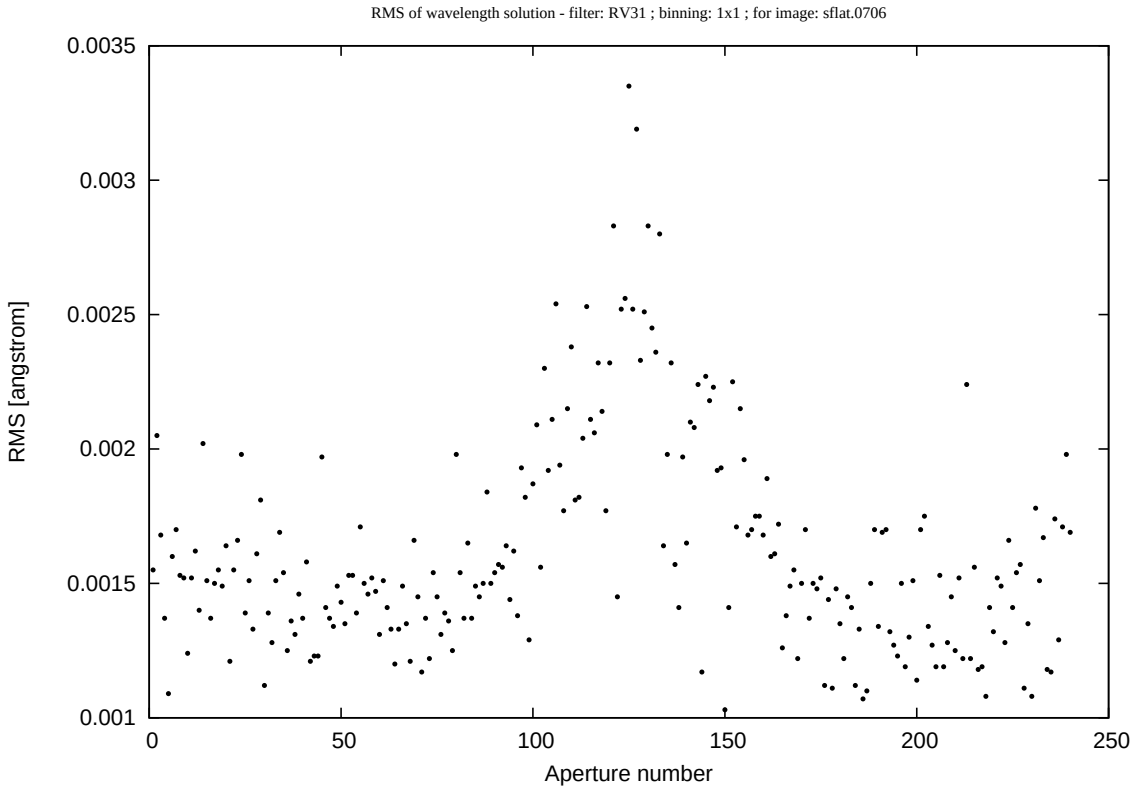

Figure 2.3: The distribution of RMS vs. aperture number for the dispersion solution from 2006.0316.

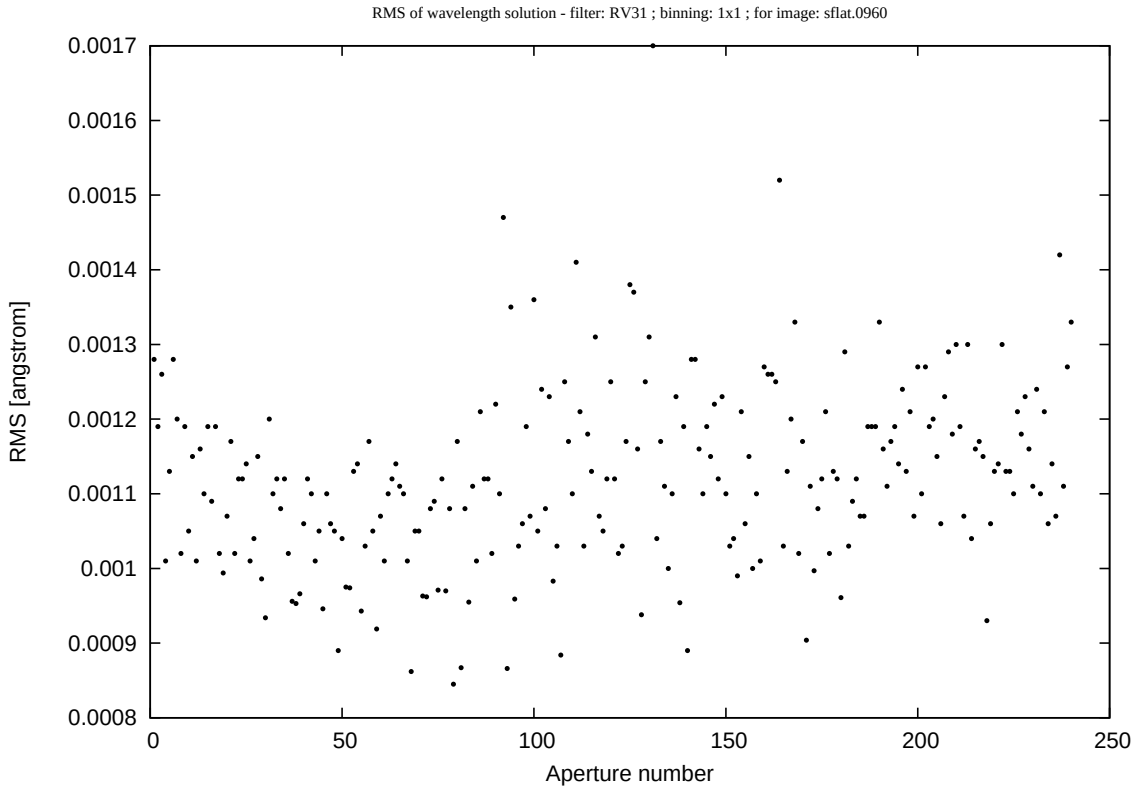

Figure 2.4: The distribution of RMS vs. aperture number for the dispersion solution from 2006.0406.

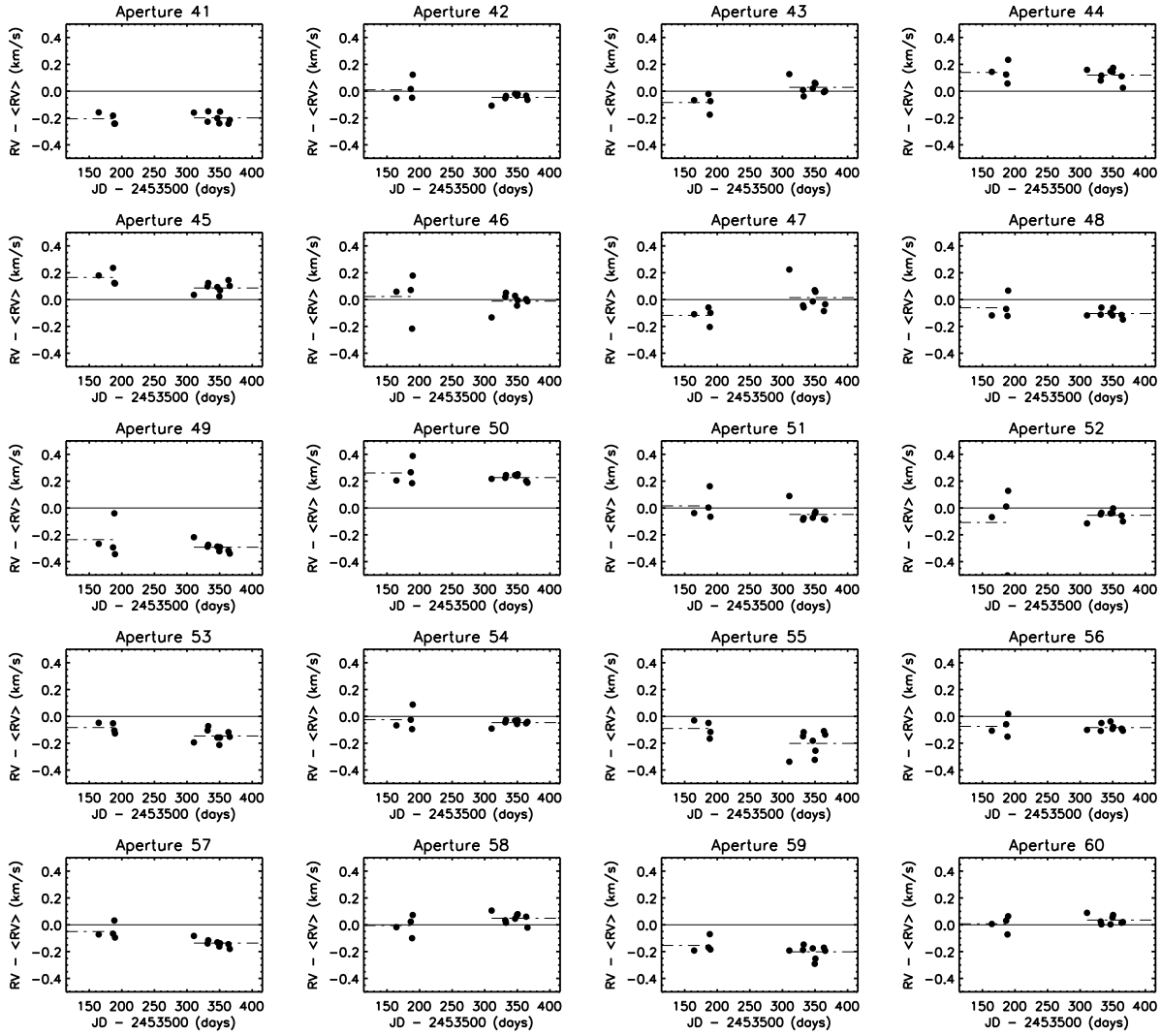

Figure 2.5: The 12 deviations (RV - $< RV >$) vs. time (MJD - 2453500) for aperture numbers 41-60.

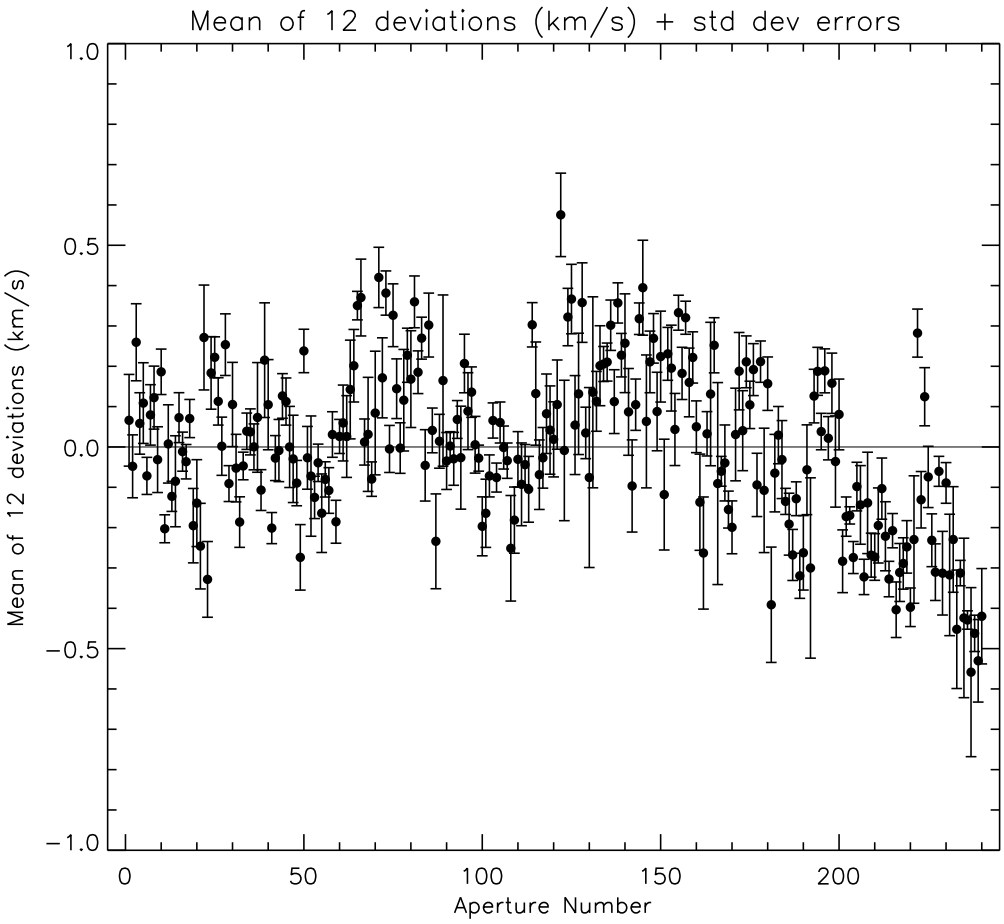

Figure 2.6: The mean of the 12 deviations for each of the 240 fibers. The errorbars represent the standard deviation of the 12 deviations.

The mean deviation for a given fiber/aperture number is presently our best determination of a correction to apply to radial velocities measured via that fiber. Note that while these mean deviations are calculated using all 12 deviations, we might want to use only deviations from data obtained after the permanent mount of the calibration lamps to the secondary. We show in Figure 2.7 and Figure 2.8 the radial velocities from all 240 fibers on all 12 afternoons corrected by the fiber-to-fiber corrections (mean deviations) shown in Figure 2.6, and by the mean offsets shown in Figure 2.2. By correcting for

the fiber-to-fiber variations we have removed largely the dependence of the velocity on the fiber/aperture number seen in Figure 2.1, and by correcting for mean offsets we have removed the night-to-night variations.

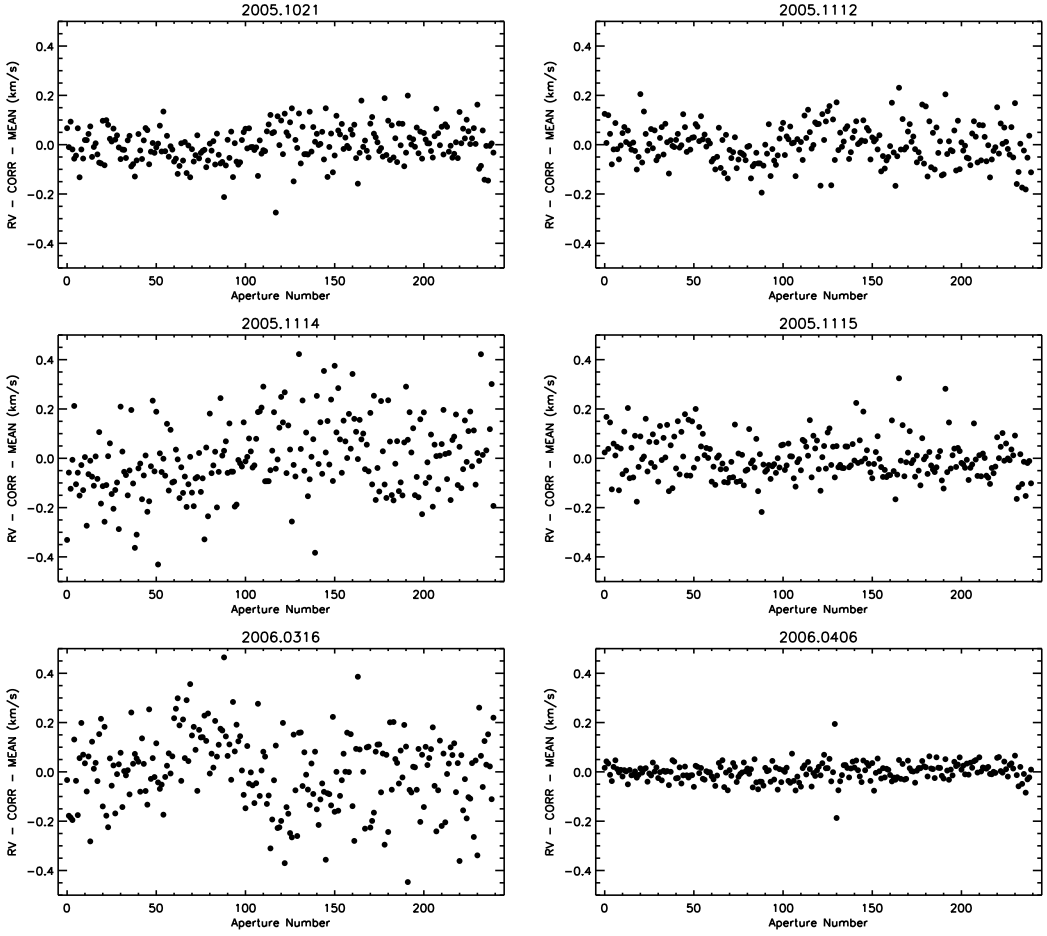

Figure 2.7: The fiber-to-fiber and night-to-night corrected radial velocities from all 240 fibers for six afternoons (2005.1021, 2005.1112, 2005.1114, 2005.1115, 2006.0316, 2006.0406).

Having corrected for the systematic fiber-to-fiber variations and the systematic night-to-night variations, we can now address the precision (repeatability) of velocity measurements for the sun in a given fiber. First, we see in Figure 2.7 and Figure 2.8 that even after the corrections are applied, there

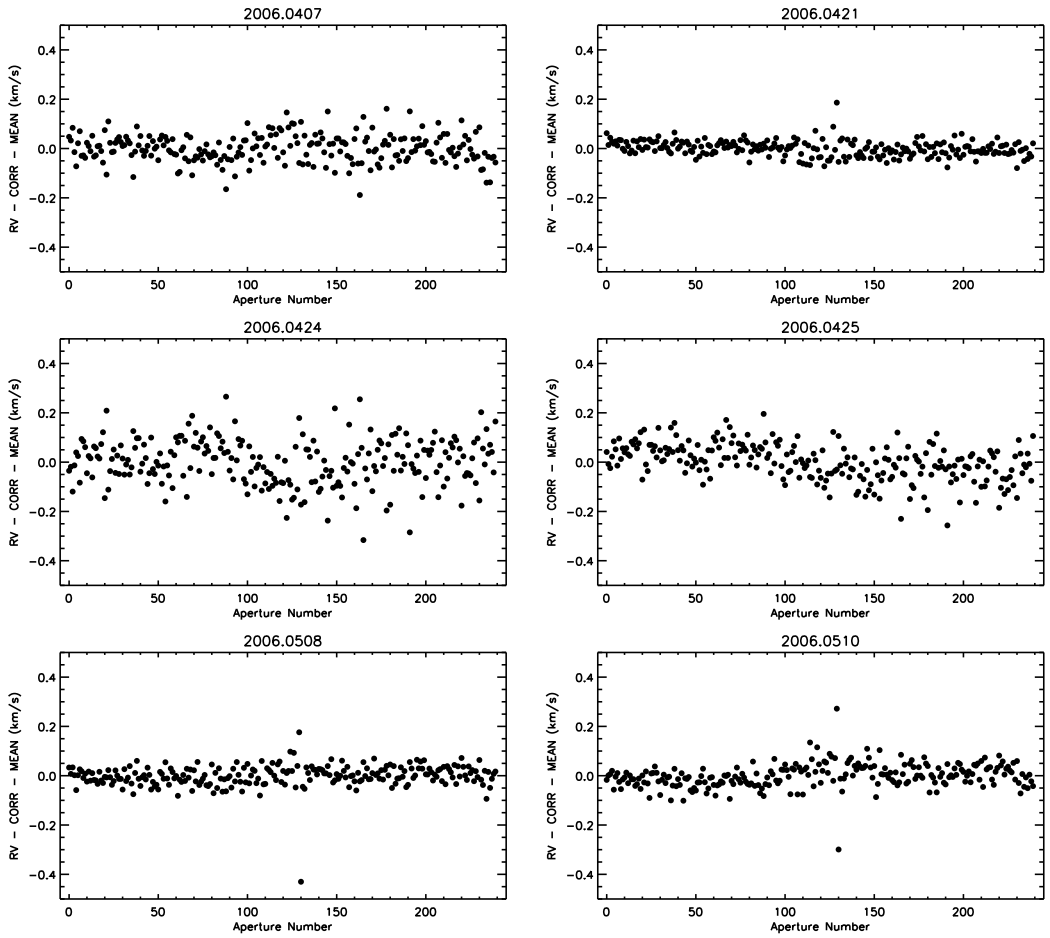

Figure 2.8: The fiber-to-fiber and night-to-night corrected radial velocities from all 240 fibers for six afternoons (2006.0407, 2006.0421, 2006.0424, 2006.0425, 2006.0508, 2006.0510).

are still lower level correlations between the velocity and the fiber/aperture number. At this level they appear to be different for different nights. In particular the difference between different afternoons in the width of the scatter around zero is intriguing. The current corrections for the fiber-to-fiber variations do not work equally well on all exposures. If we can figure out what is different from afternoon to afternoon and thereby achieve results as for 2006.0406 and 2006.0421, we could potentially gain of order 100 m/s in the

RV precision.

Figures 2.9 and 2.10 show the distributions of the differences between the velocity deviations of individual fibers from the exposure mean (FTF) and the means of 12 such deviations from the 12 afternoon skies ($< FTF >$). Each histograms is labeled with the date of the afternoon sky-exposure from which the velocity deviations (FTF) were determined. When comparing to Figures 2.7 and 2.8 it is clear that narrow distributions centered most closely on zero in Figures 2.9 and 2.10, correspond to the most narrow and flat distributions of corrected solar velocities in Figures 2.7 and 2.8. This correlation tells us that the varying quality of the corrections displayed in Figures 2.7 and 2.8 are due to an increasing and decreasing mismatch between the mean fiber-to-fiber corrections applied and the actual velocity deviations on a given afternoon. For now the conclusion must be that nightly variations in the deviations from the exposure mean of individual fibers, are at a level above the radial velocity precision we would like to achieve. The results presented here thus suggest that we must aquire calibration data on a daily basis that will allow us to correct for the nightly fiber-to-fiber variations as best possible.

As a measure of how precisely we currently can measure the velocity of the sun after corrections for solar-systems dynamics, fiber-to-fiber variations, and night-to-night variations, we show in Figure 2.11 and in Figure 2.12 the standard deviation and the standard error on the mean, respectively, of the 12 velocities for a given fiber.

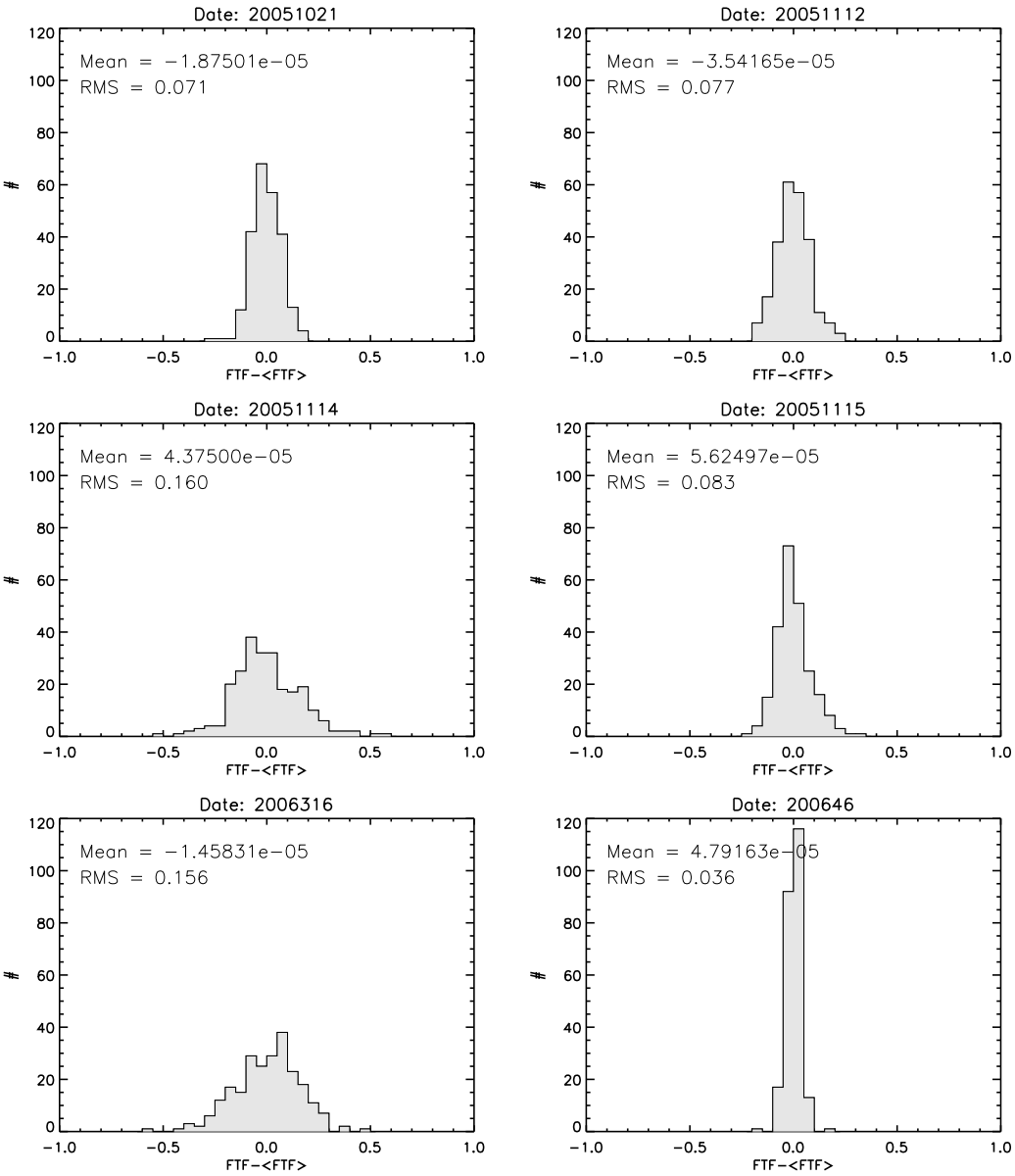

Figure 2.9: Distributions of the differences between velocity deviations of individual fibers from the exposure mean (FTF) and the means of 12 such deviations from the 12 afternoon skies ($< FTF >$). Each histograms is labeled with the date of the afternoon sky-exposure from which the velocity deviations (FTF) were determined.

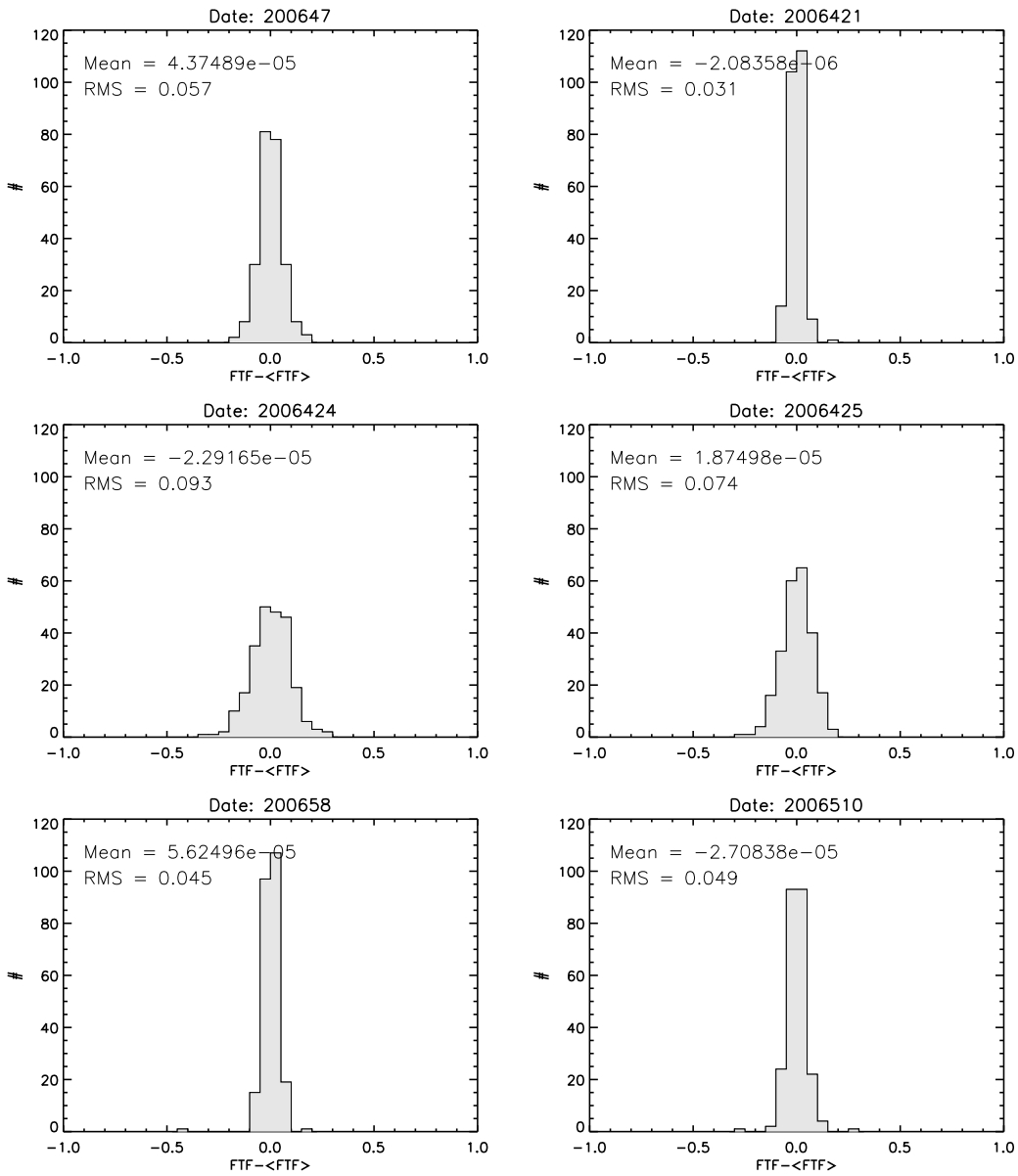

Figure 2.10: Distributions of the differences between velocity deviations of individual fibers from the exposure mean (FTF) and the means of 12 such deviations from the 12 afternoon skies ($< FTF >$). Each histograms is labeled with the date of the afternoon sky-exposure from which the velocity deviations (FTF) were determined.

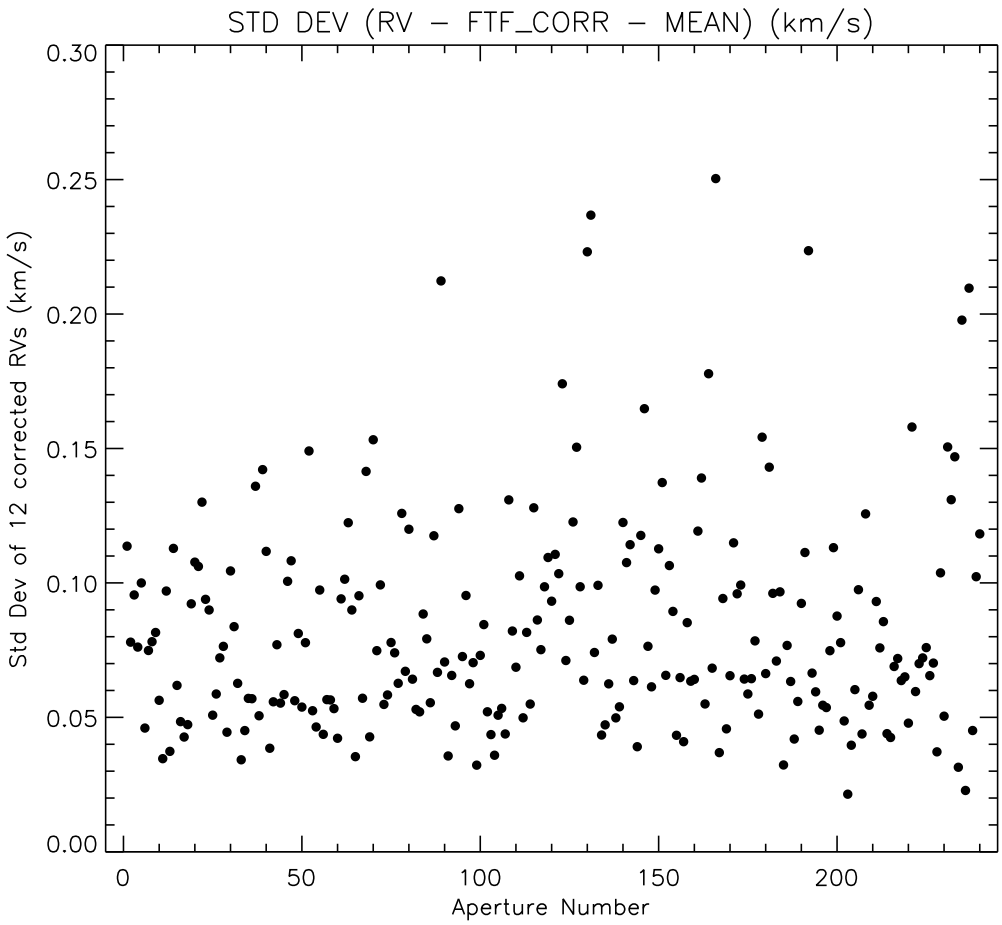

Figure 2.11: The standard deviation of the 12 corrected solar velocities for the 240 fibers.

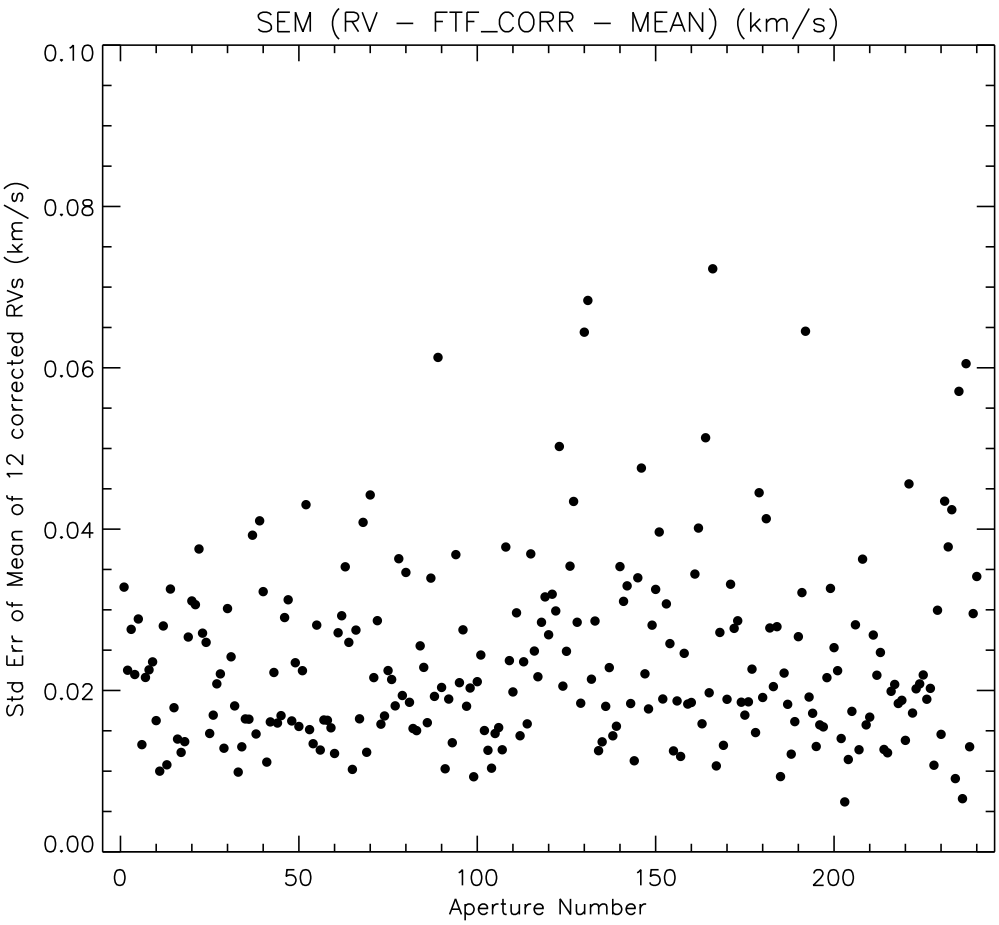

Figure 2.12: The standard error on the mean of the 12 corrected solar velocities for the 240 fibers.

Chapter 3

M67 - observations, data-reduction, and analysis

3.1 Goal

To test the accuracy of corrected MMT/Hectochelle radial velocities by measuring the velocities of a sample of high probability single stars in M67 for which several epoch of velocities exist from the CfA survey using the 60 inch and the CfA speedometer.

3.2 Data used

The calibration and M67 science exposures used here were obtained on the night of 2005.1115. Table 3.1 list relevant information for these exposures.

Table 3.1: 2005.1115 M67 science and calibration exposures used.

Date	Type	Filename	Order	t_{exp}	Lamp mount	Fiber conf.
2005.1115	ThAr	comp.0800	RV31	600	manlifter	ring200
2005.1115	ThAr	comp.0819	RV31	900	manlifter	ring200
2005.1115	DF	domeflat.0793	RV31	1.0	manlifter	ring200
2005.1115	DF	domeflat.0794	RV31	1.0	manlifter	ring200
2005.1115	DF	domeflat.0795	RV31	1.0	manlifter	ring200
2005.1115	SF	sflat.0801	RV31	1	manlifter	ring200
2005.1115	SF	sflat.0802	RV31	10	manlifter	ring200
2005.1115	SF	sflat.0803	RV31	15	manlifter	ring200
2005.1115	SF	sflat.0804	RV31	20	manlifter	ring200
2005.1115	SF	sflat.0805	RV31	60	manlifter	ring200
2005.1115	SF	sflat.0806	RV31	75	manlifter	ring200
2005.1115	SF	sflat.0807	RV31	90	manlifter	ring200
2005.1115	SF	sflat.0808	RV31	110	manlifter	ring200
2005.1115	SF	sflat.0809	RV31	130	manlifter	ring200
2005.1115	Science	M67_stab_test_1.0863	RV31	600	manlifter	M67_stab_test
2005.1115	Science	M67_stab_test_1.0864	RV31	600	manlifter	M67_stab_test
2005.1115	DF	domeflat.0865	RV31	1 manlifter	M67_stab_test	
2005.1115	ThAr	comp.0866	RV31	720 manlifter	M67_stab_test	

3.3 Velocity corrections applied

The 2005.1115 afternoon calibration data listed in Table 3.1 provide a nightly offset (-152.8 m/s) measured as the offset from zero of the mean of the 240 velocities from the afternoon sky-exposure (see Chapter 2 and Figure 2.2). The deviations of the 240 velocities from the mean provide a set of fiber-to-fiber variations specifically for 2005.1115, while a general set of fiber-to-fiber variations was calculated in Chapter 2 as the mean of the fiber-to-fiber variations from 12 separate afternoons. In what follows we will correct the derived radial velocities in M67 for the nightly offset and for the specific or general fiber-to-fiber variations, respectively.

Furthermore, because a correction for the gavitational redshift of the solar radiation ($-636km/s$) was applied to all sky-velocities used in Chapter 2 to derive nightly offsets, the same correction is applied to the derived M67 velocities. In addition, the M67 radial velocities to which we will compare our velocities, have a known 139 m/s offset, in the sense that 139 m/s needs to be added to the CfA velocities to put them on an absolute scale. Accordingly we have added 139 m/s to the CfA velocities before comparison with our MMT/Hectochelle velocities.

3.4 M67 Radial-Velocity Histogram

Figure 3.1 shows the radial-velocity distributions for approximately 160 stars from the MMT/Hectochelle M67 pointing. The vertical solid lines represent a crude velocity cluster membership criteria, and the values for the mean, median, standard deviation, and FWHM listed, are based on the stars that fall between these lines. In the top panel the histogram represent velocities corrected with the mean fiber-to-fiber variations, while in the bottom panel the velocities were corrected with the fiber-to-fiber deviations from the afternoon of 2005.1115.

3.5 Comparison between absolute CfA speedometer and MMT/Hectochelle velocities

In Figure 3.2 we display the difference between the CfA Speedometer and the Hectochelle radial velocities for 65 single lined members in M67. The

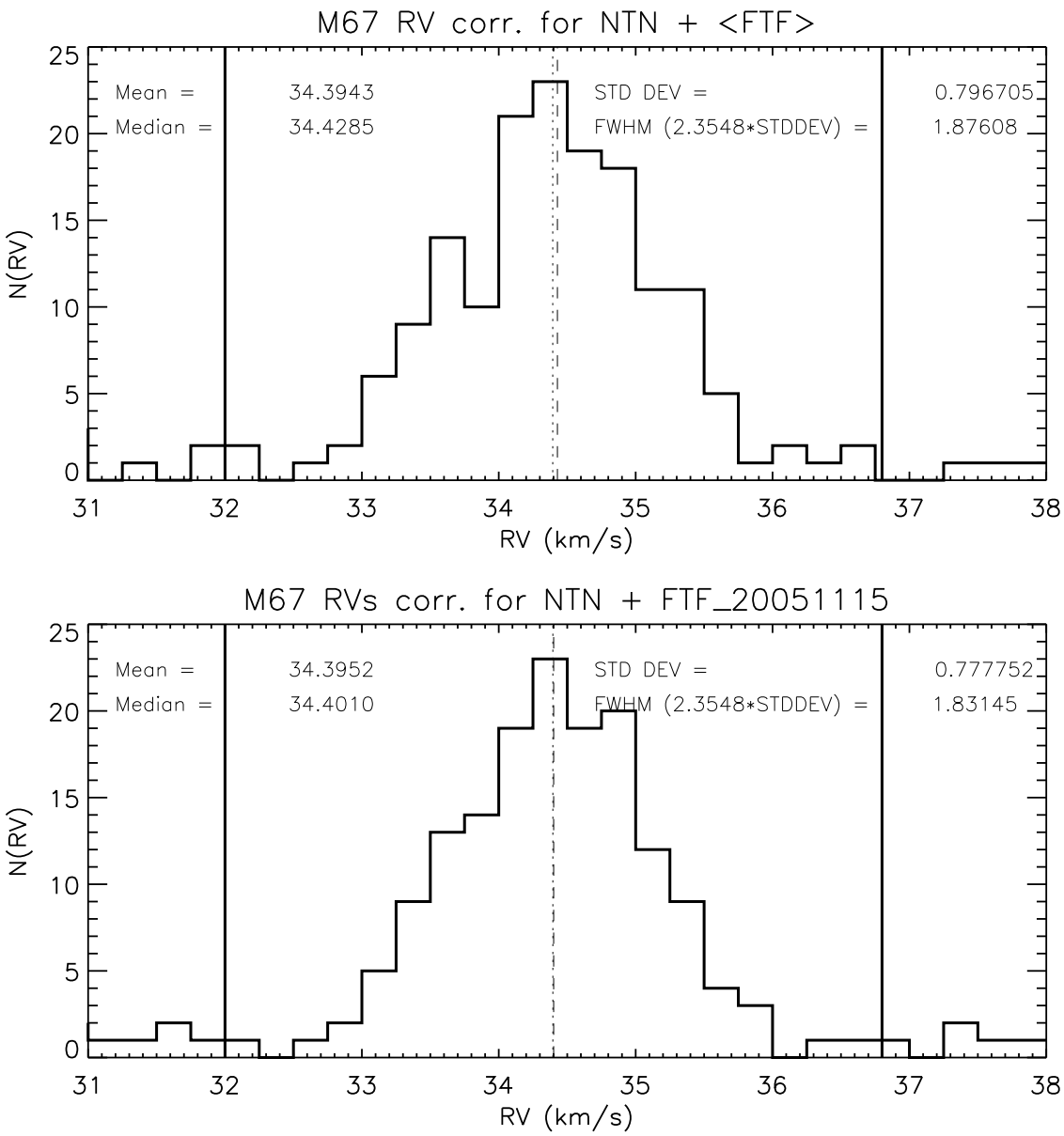

Figure 3.1: The radial-velocity distributions approximately 160 stars from the MMT/Hectochelle M67 pointing. Listed values for the mean, median, standard deviation, and FWHM are for stars that fall between the vertical solid lines. Top histogram represent velocities corrected with the mean fiber-to-fiber variations. Bottom histogram represent velocities corrected with the fiber-to-fiber deviations from the afternoon of 2005.1115.

three panels each represent Hectochelle velocities with either no corrections applied (top), nightly correction and mean fiber-to-fiber corrections applied (center), and nightly correction and 2005.1115 fiber-to-fiber corrections applied (bottom). In each panel the mean difference and the RMS of the 65 differences are listed. Two stars at the faint end ($V > 14$) fall beyond the region shown here with differences of 3.46 and -6.85 km/s.

As is likely the case for the latter two M67 stars, many of the stars shown in Figure 3.2 are likely long period single lined binaries. In an attempt to consider only single stars, or at least minimize the contamination from binary stars, we looked for an overlap between the 65 stars shown in Figure 3.2 and the list of high-probability single members published by Sandquist (2004). There were 29 stars in common between the two lists, and Figure 3.3 shows as in Figure 3.2 the radial-velocity differences between the CfA Speedometer and the Hectochelle radial velocities for the 29 high-probability single members of M67.

While the mean differences seen in Figures 3.2 and 3.3 are encouraging, the individual differences for more than half of the 29 stars are too large if they are indeed single members. We must look more carefully at the number of observations, the time baseline, quality of correlations etc for a number of these stars to try to understand these large differences.

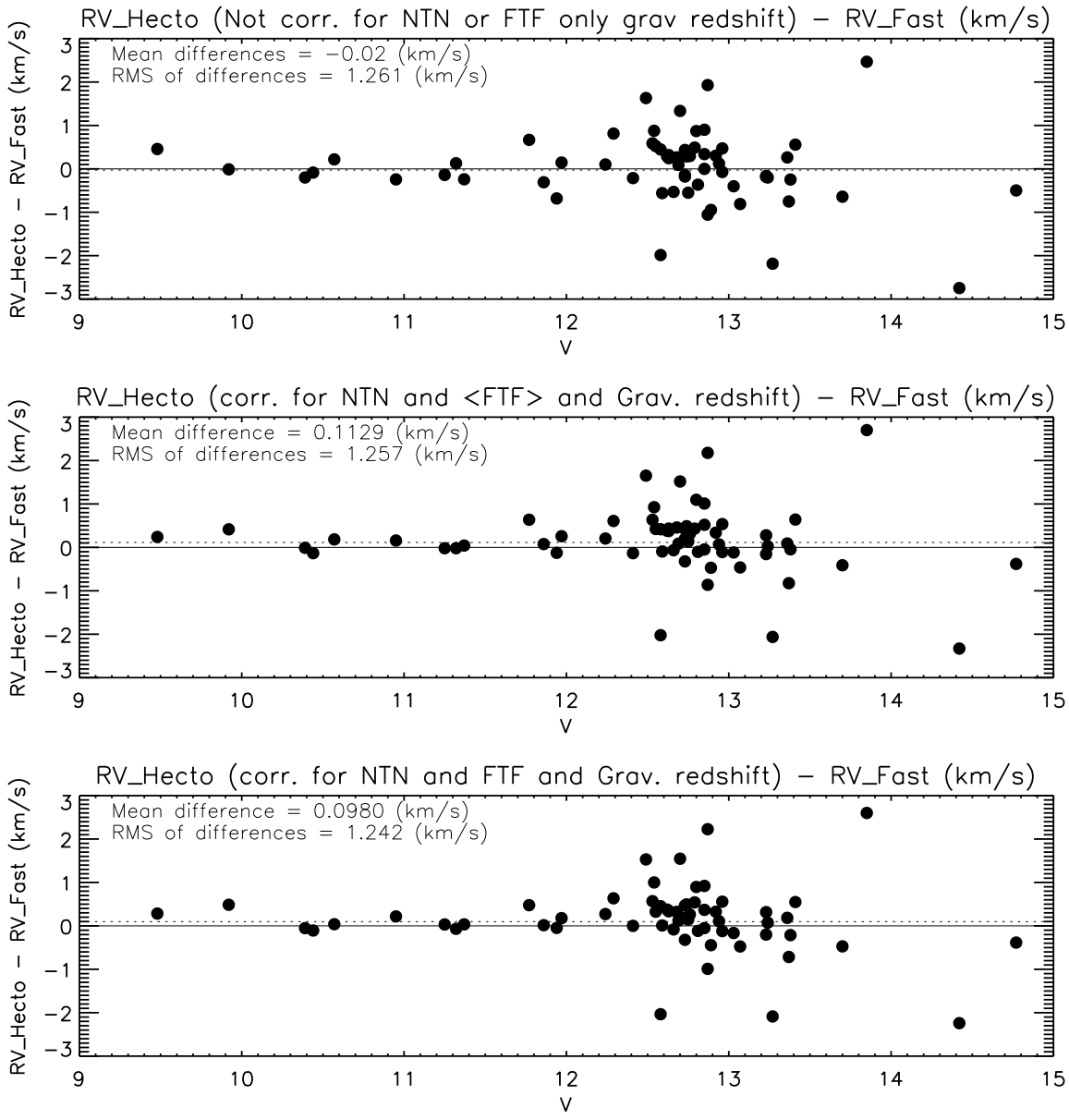

Figure 3.2: The differences between CfA Speedometer and the Hectochelle radial velocities as a function of V magnitude for 65 single lined members in M67.

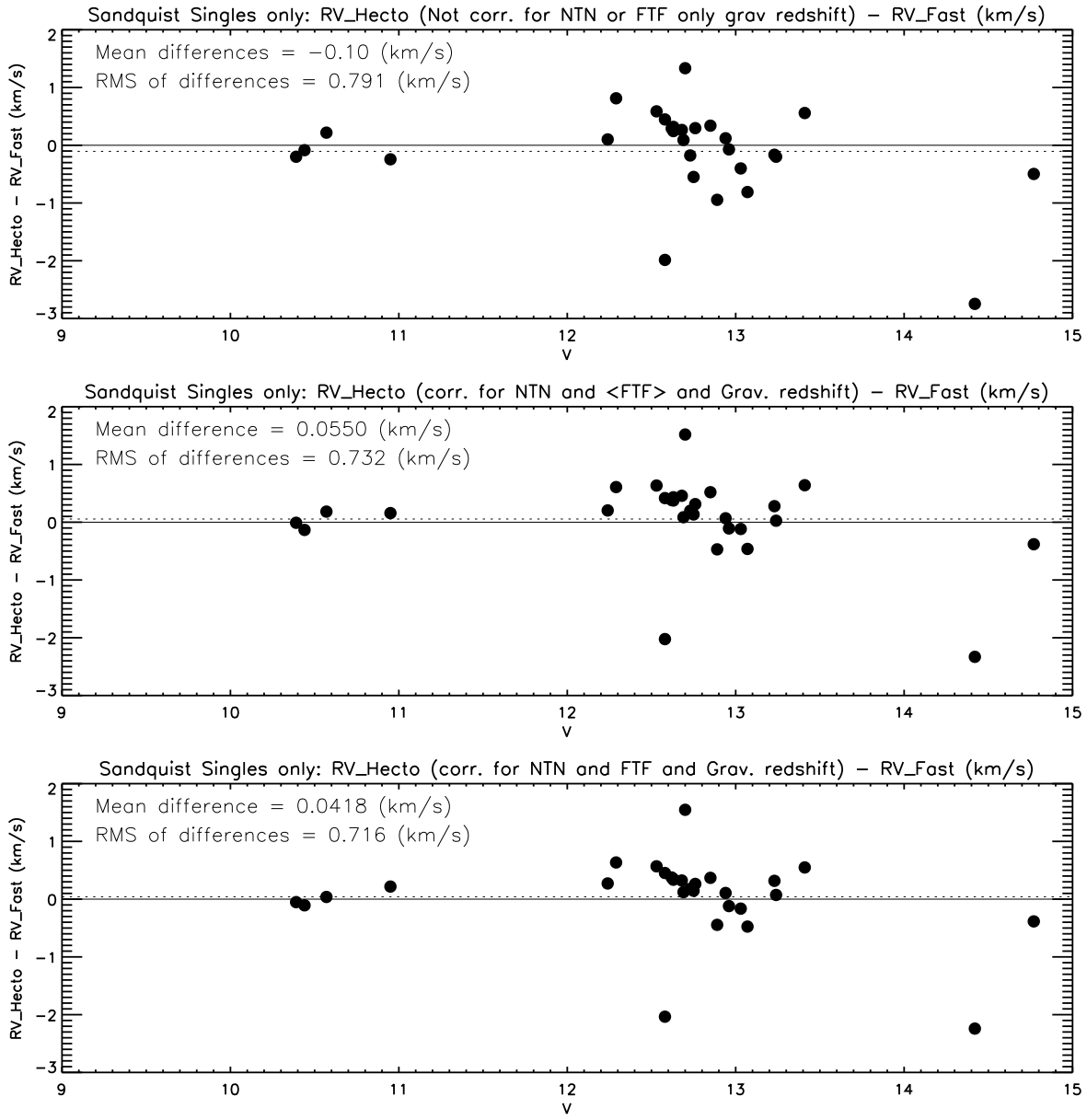

Figure 3.3: The differences between CfA Speedometer and the Hectochelle radial velocities as a function of V magnitude for 29 high-probability single members published by Sandquist (2004).

Appendix A

Relative velocity deviations with time for individual fibers/apertures

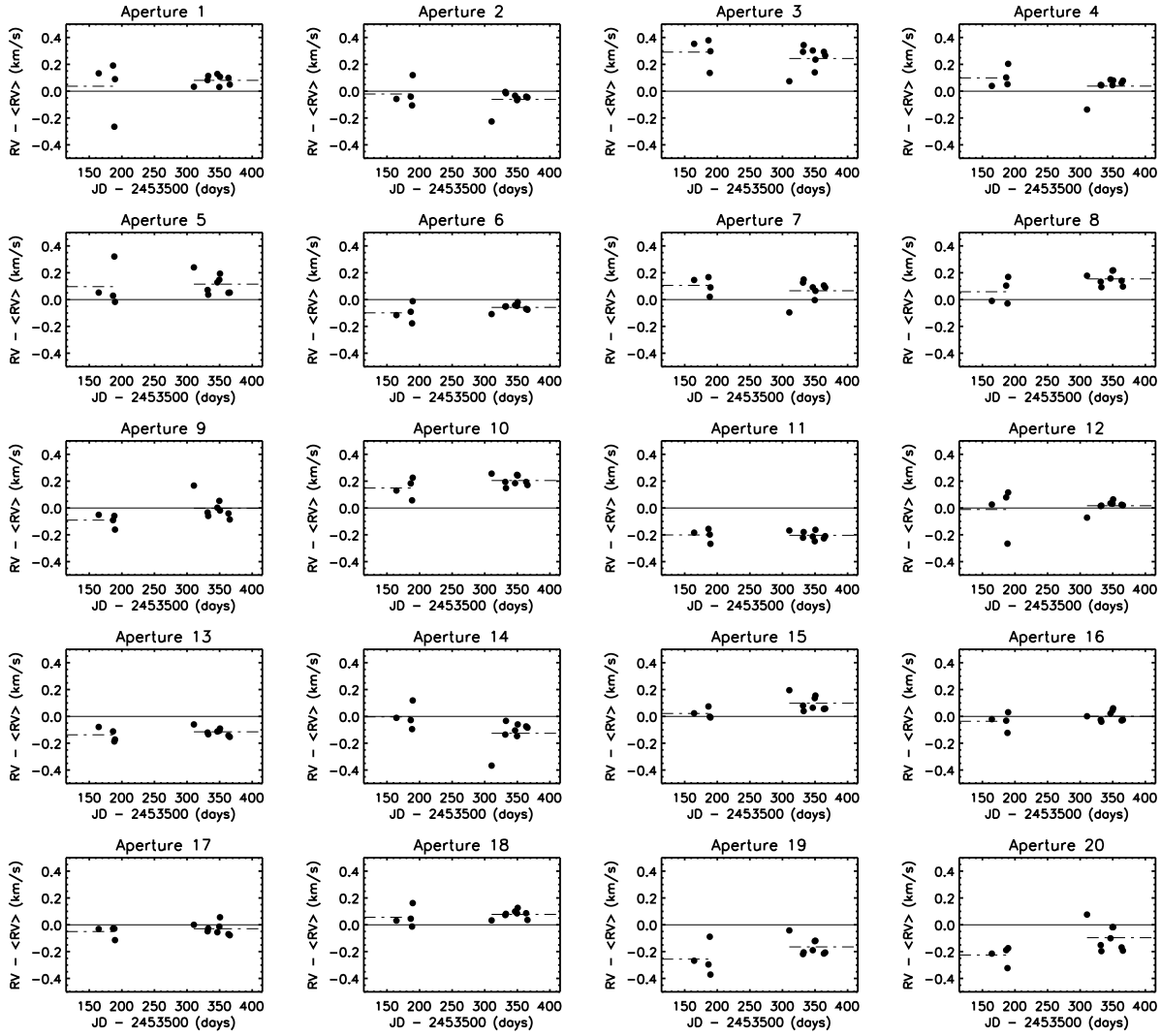

Figure A.1: The 12 deviations (RV - $< RV >$) vs. time (MJD - 2453500) for aperture numbers 1-20.

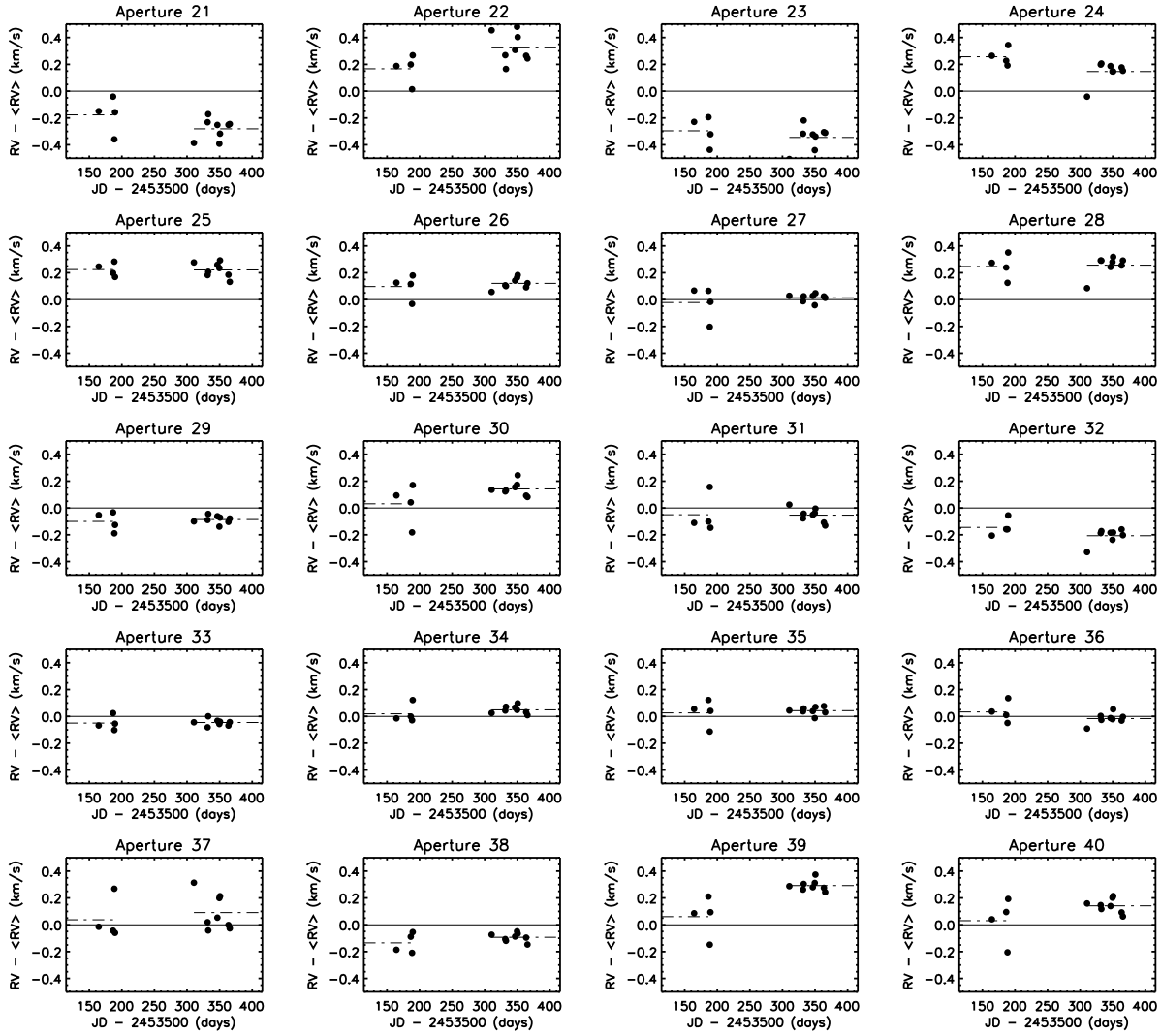

Figure A.2: The 12 deviations (RV - $< RV >$) vs. time (MJD - 2453500) for aperture numbers 21-40.

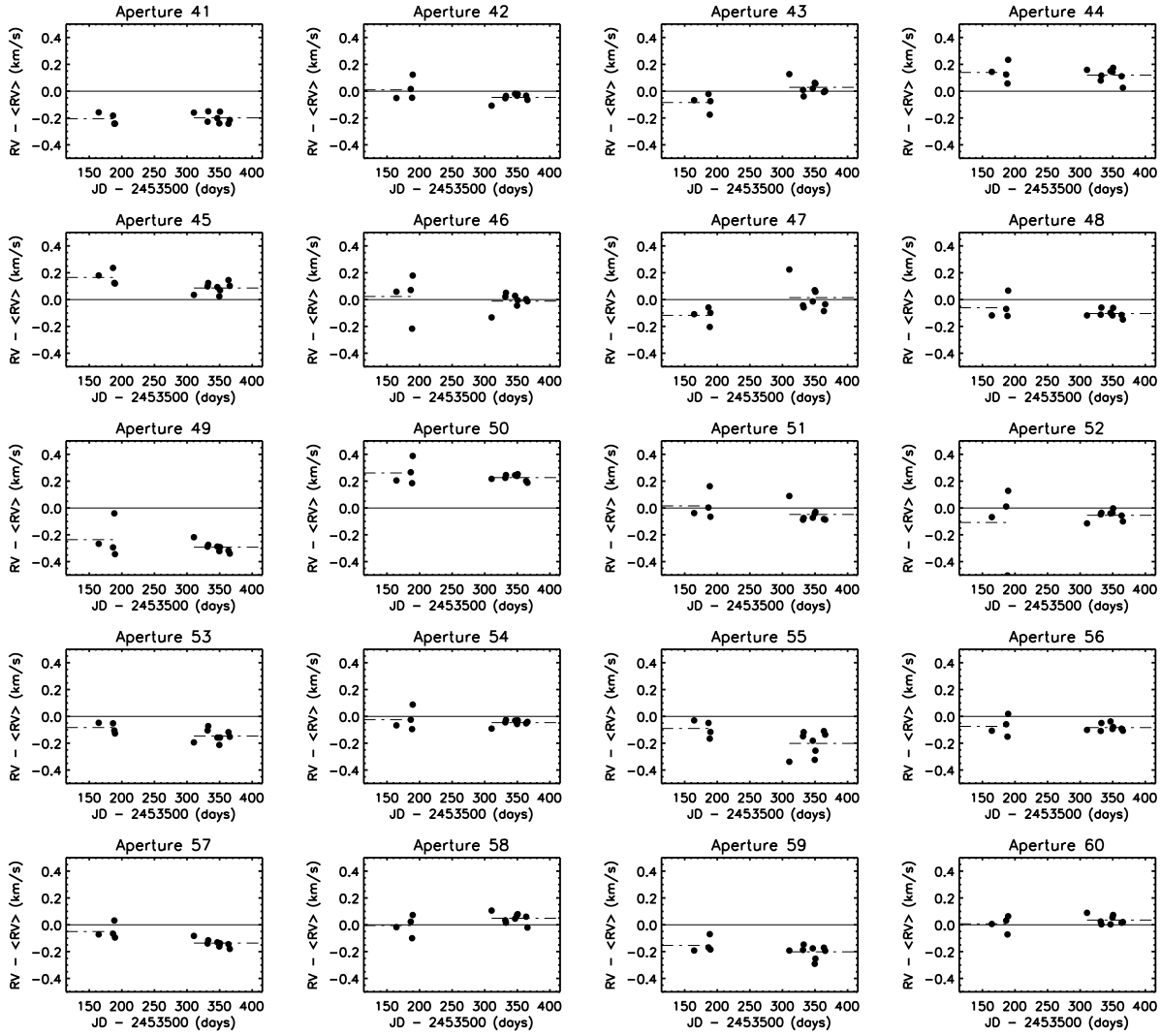

Figure A.3: The 12 deviations (RV - $< RV >$) vs. time (MJD - 2453500) for aperture numbers 41-60.

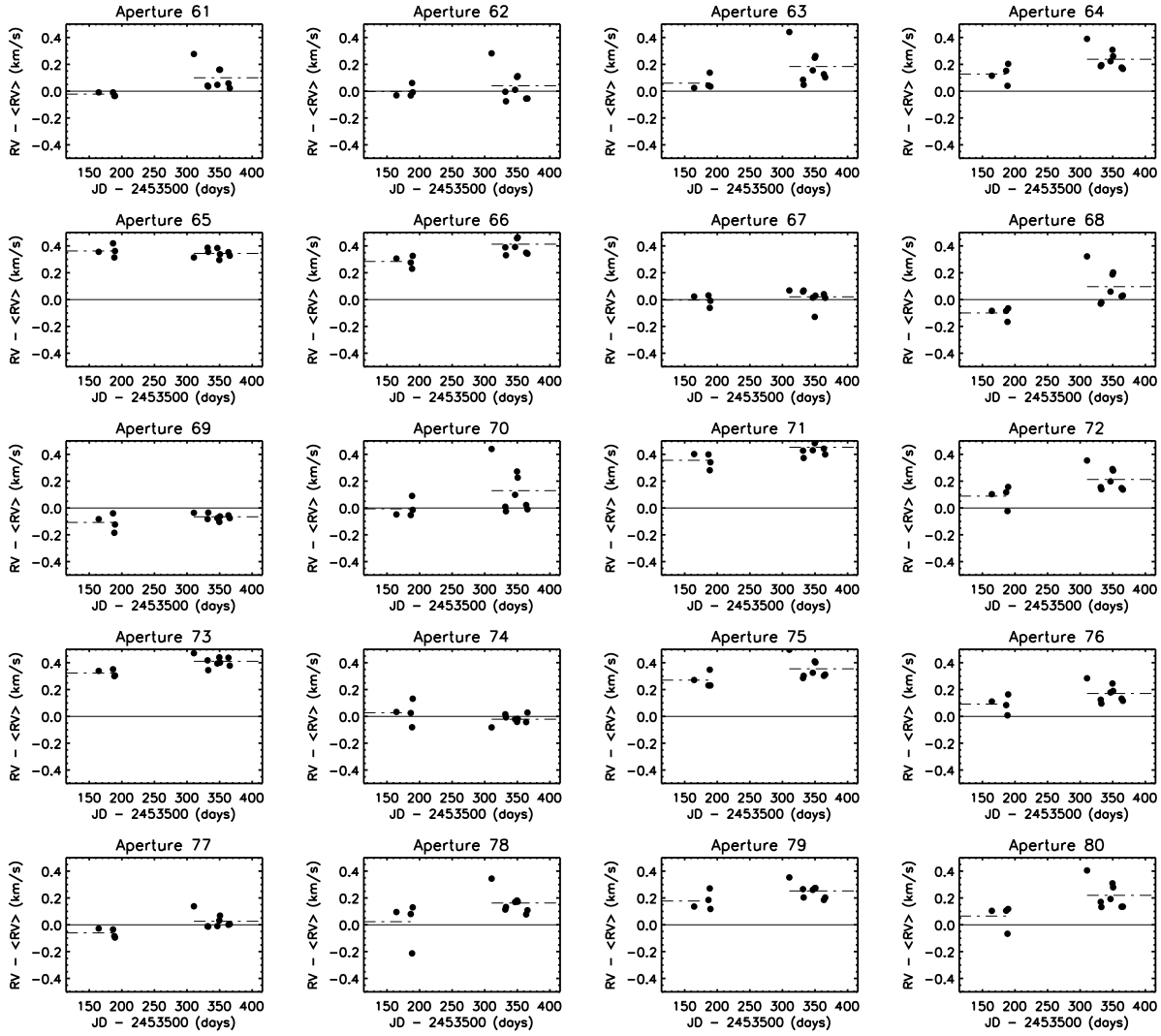

Figure A.4: The 12 deviations (RV - $< RV >$) vs. time (MJD - 2453500) for aperture numbers 61-80.

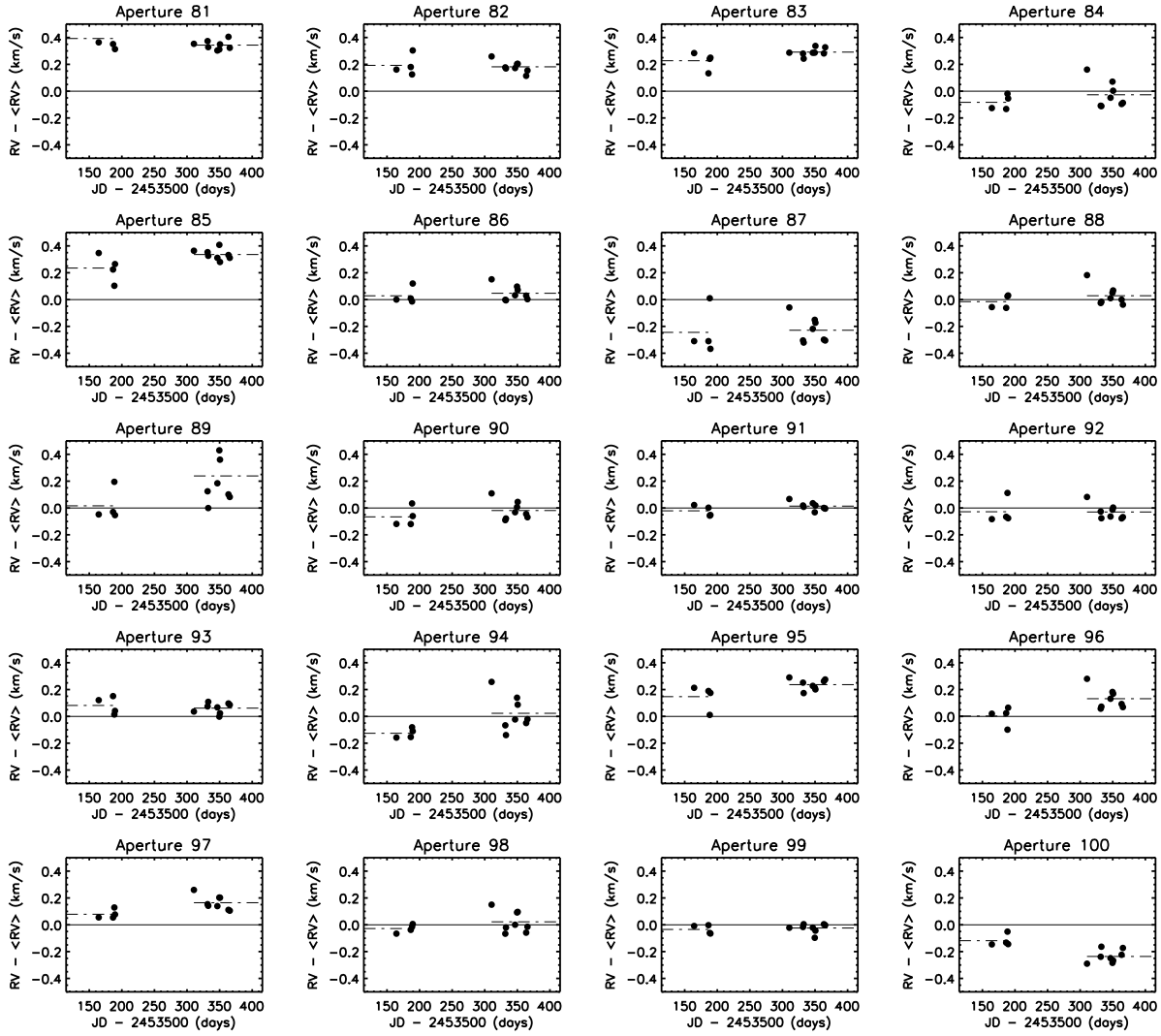

Figure A.5: The 12 deviations (RV - $< RV >$) vs. time (MJD - 2453500) for aperture numbers 81-100.

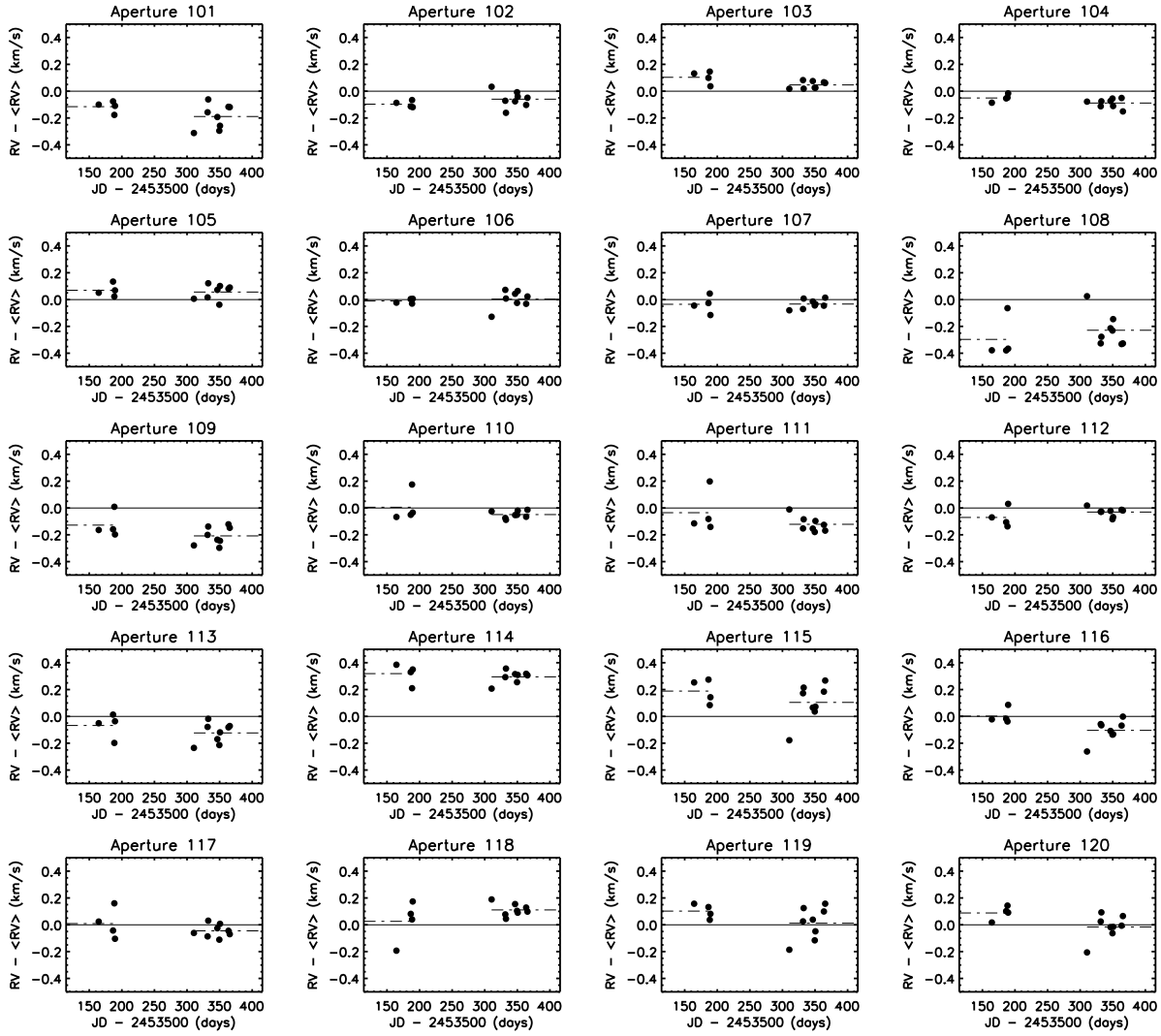

Figure A.6: The 12 deviations (RV - $< RV >$) vs. time (MJD - 2453500) for aperture numbers 101-120.

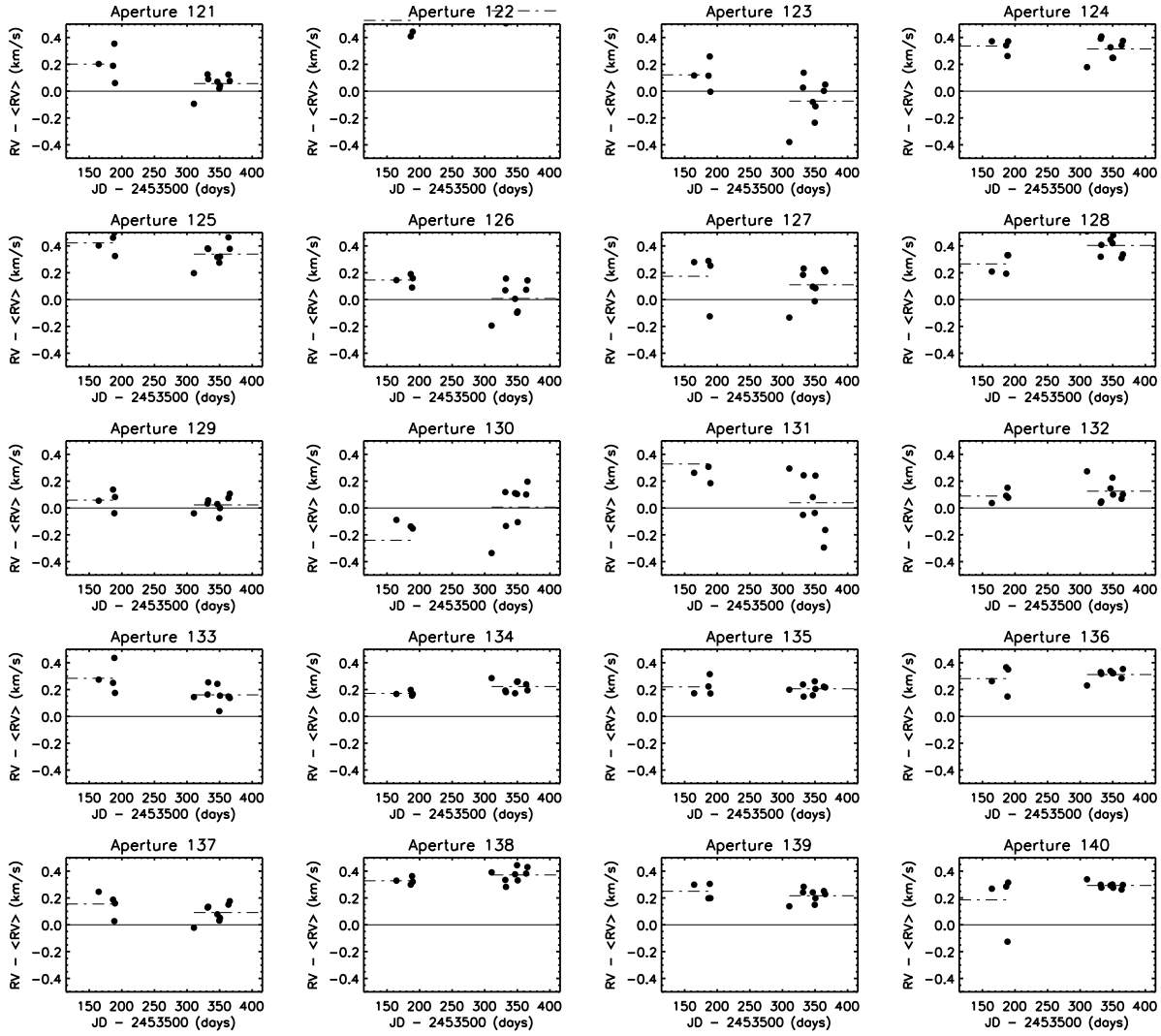

Figure A.7: The 12 deviations (RV - $< RV >$) vs. time (MJD - 2453500) for aperture numbers 121-140.

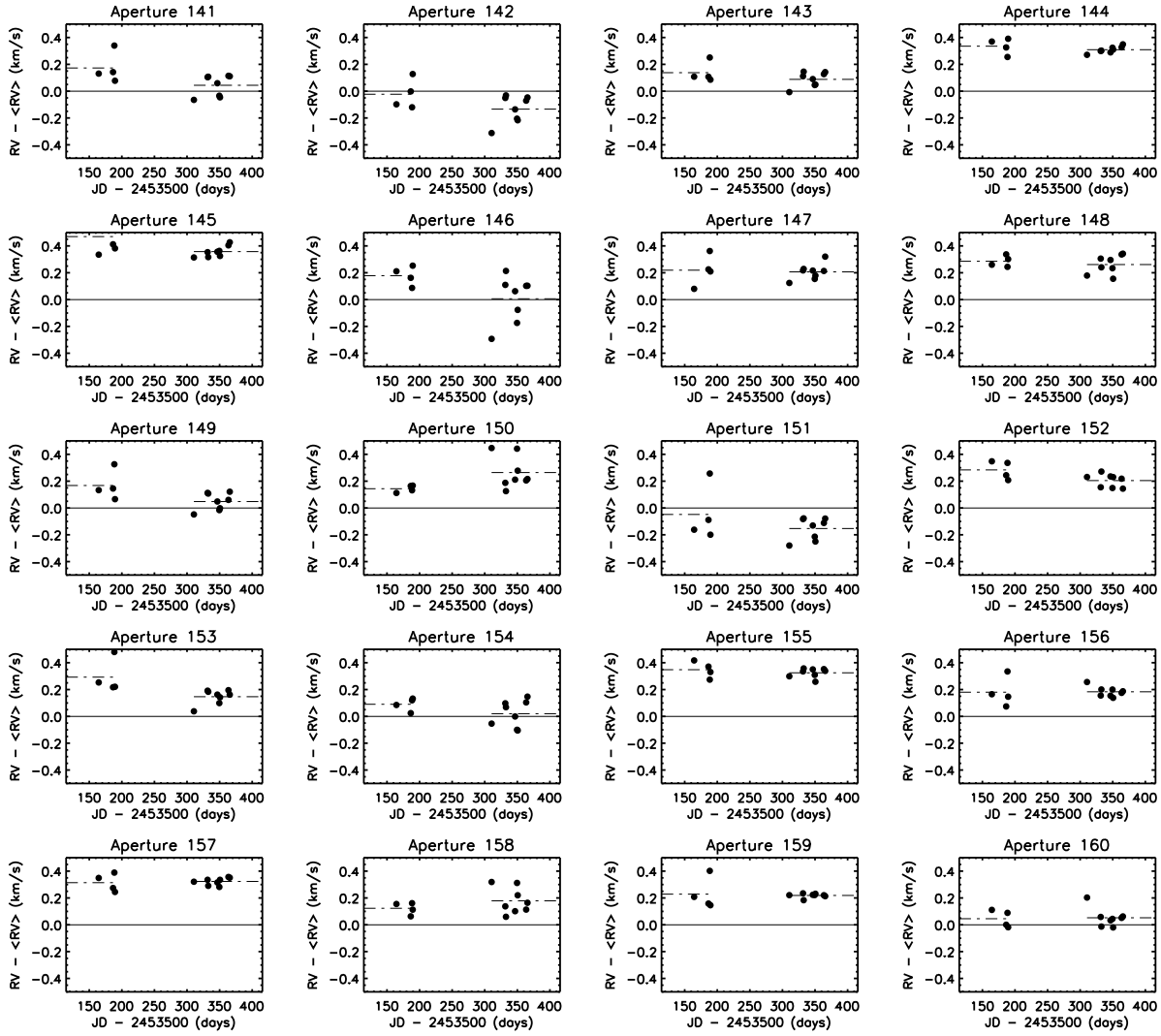

Figure A.8: The 12 deviations (RV - $< RV >$) vs. time (MJD - 2453500) for aperture numbers 141-160.

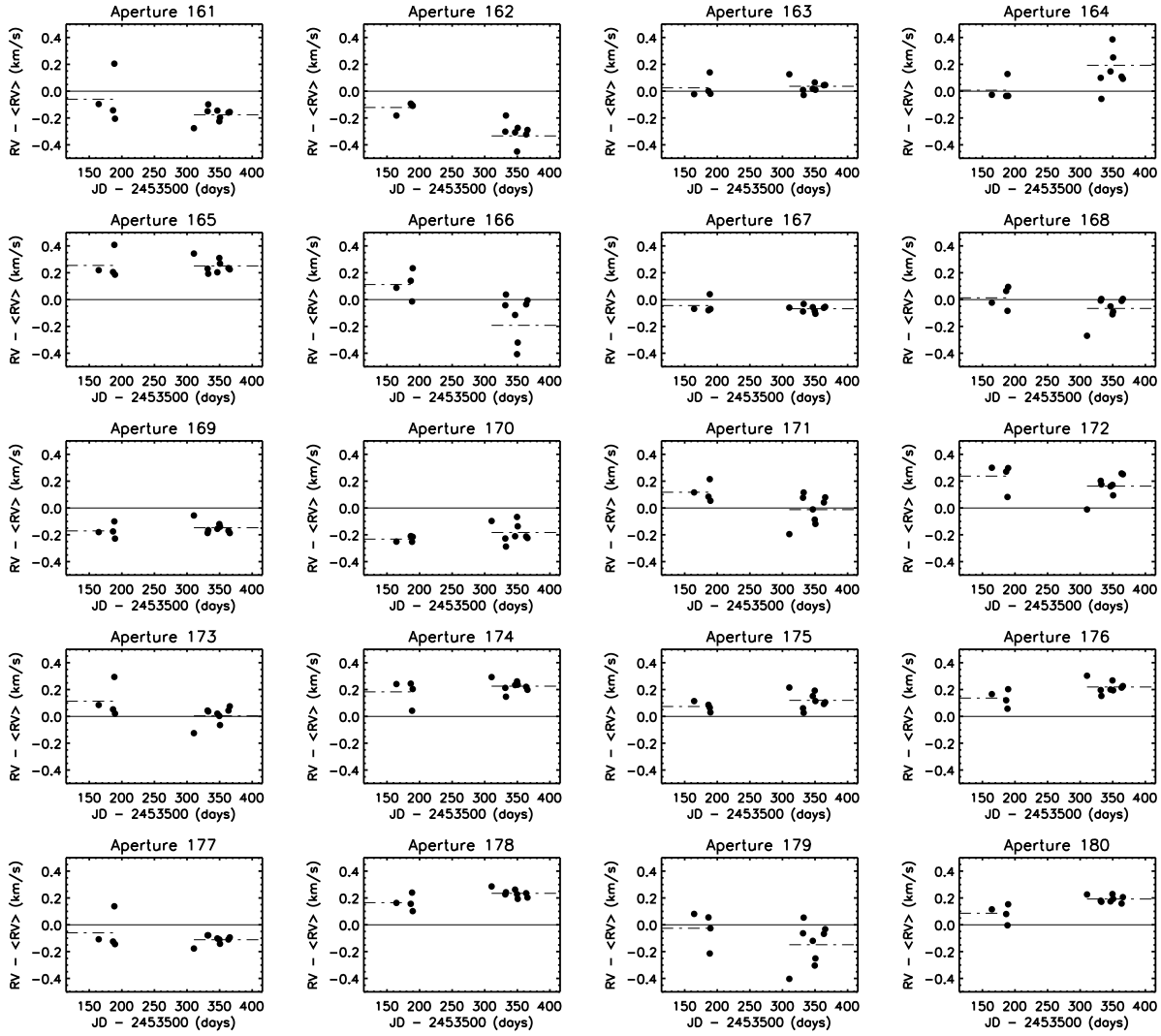

Figure A.9: The 12 deviations (RV - $< RV >$) vs. time (MJD - 2453500) for aperture numbers 161-180.

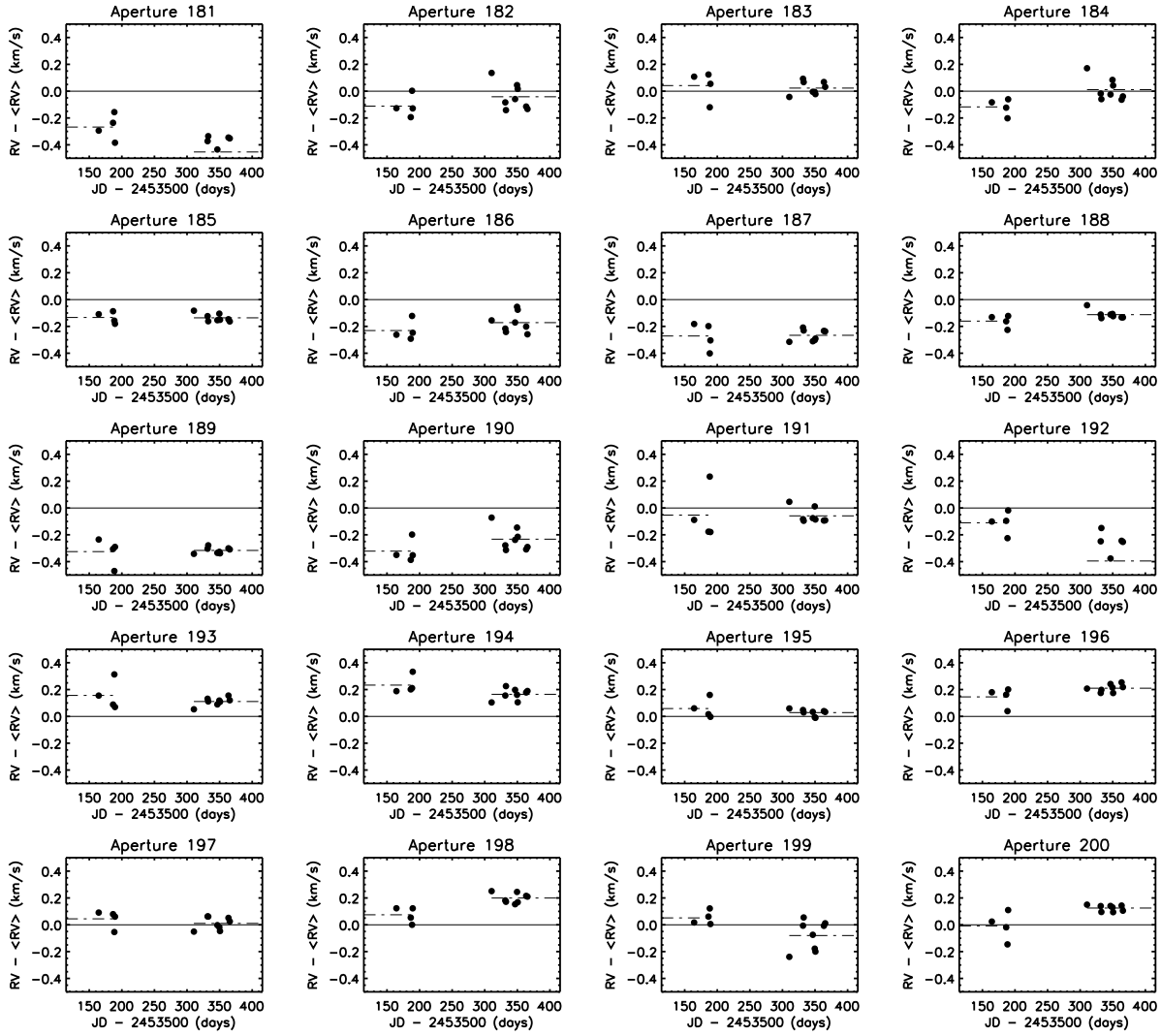

Figure A.10: The 12 deviations (RV - $< RV >$) vs. time (MJD - 2453500) for aperture numbers 181-200.

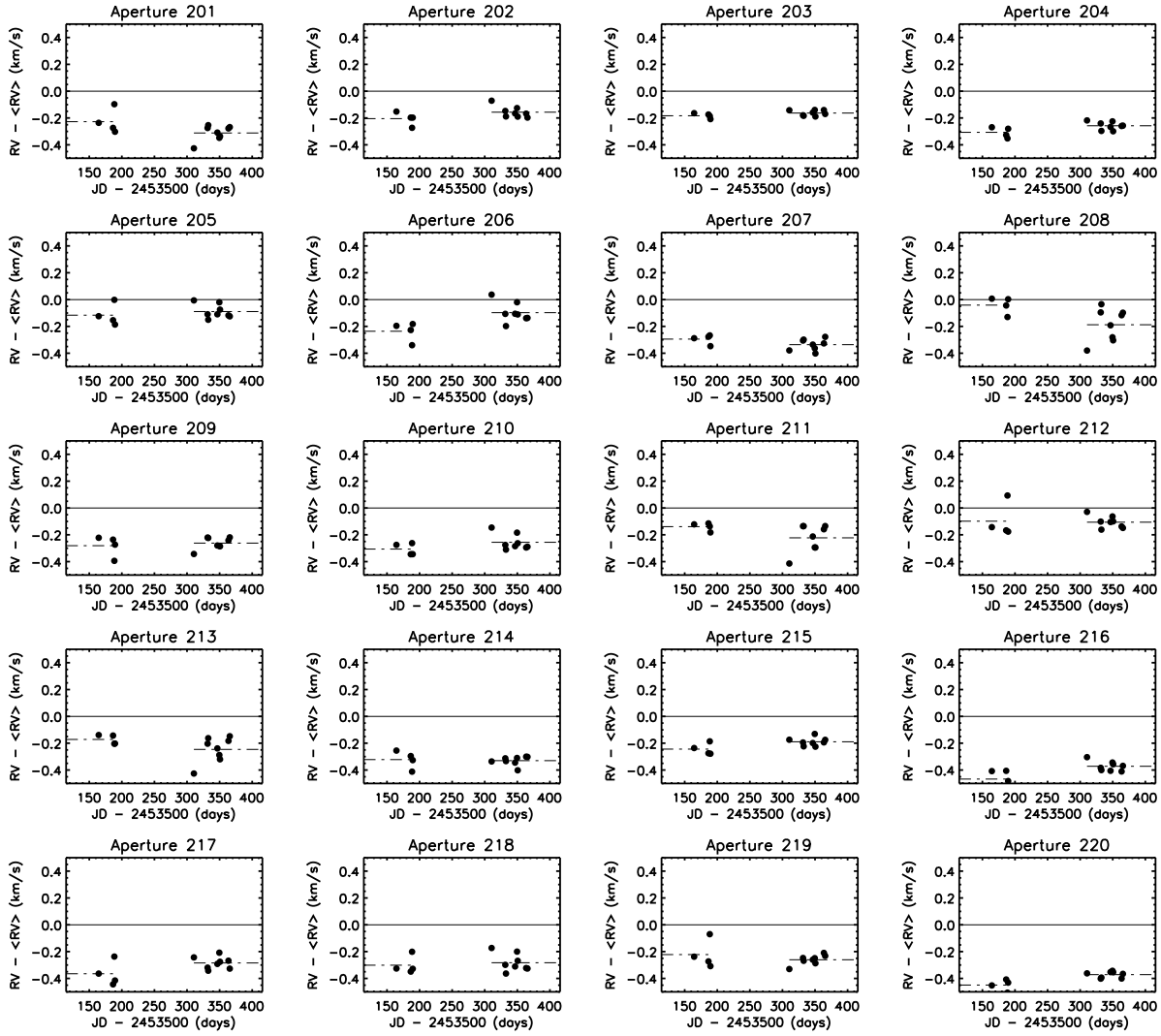

Figure A.11: The 12 deviations (RV - $< RV >$) vs. time (MJD - 2453500) for aperture numbers 201-220.

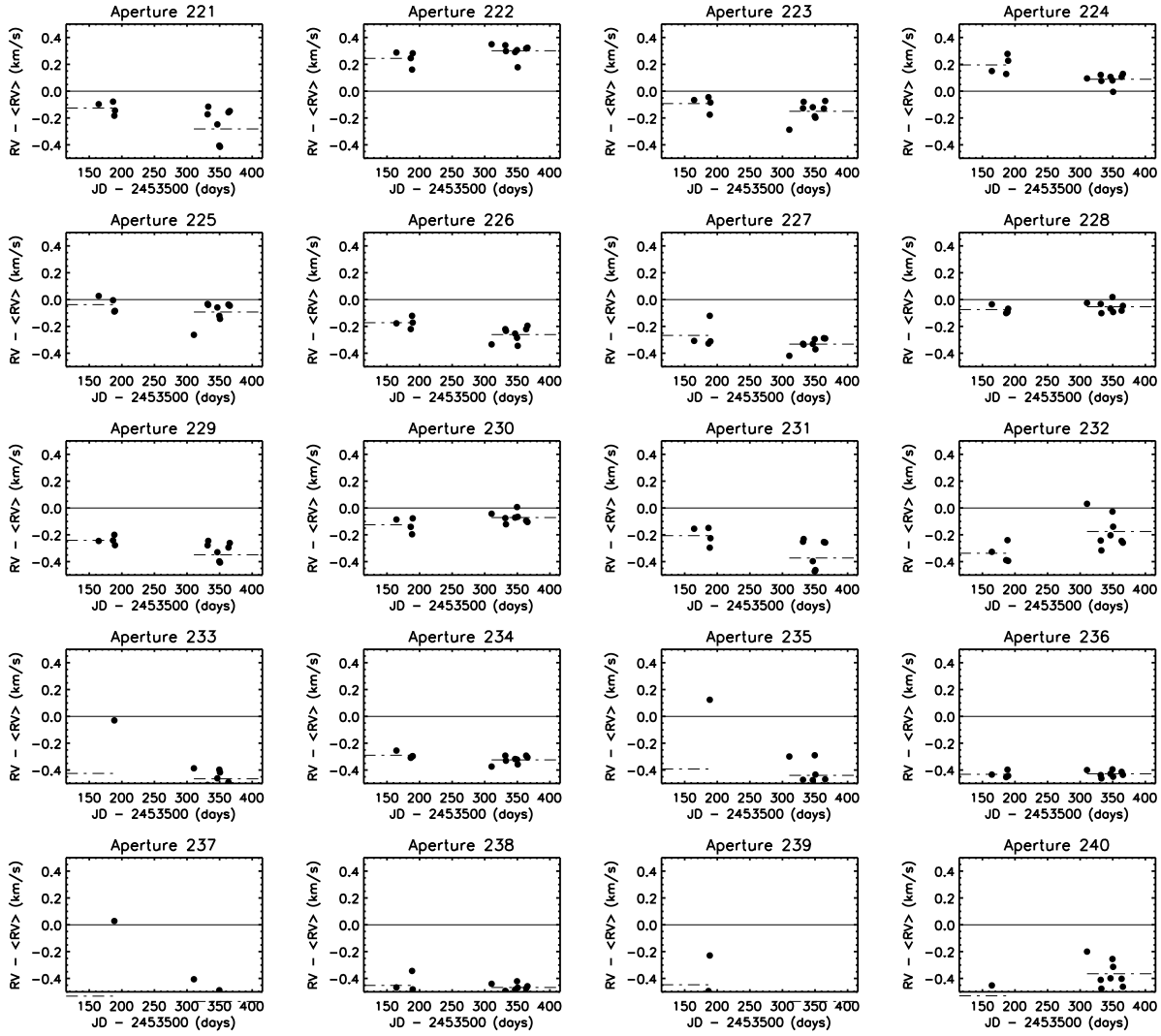

Figure A.12: The 12 deviations (RV - $< RV >$) vs. time (MJD - 2453500) for aperture numbers 221-240.

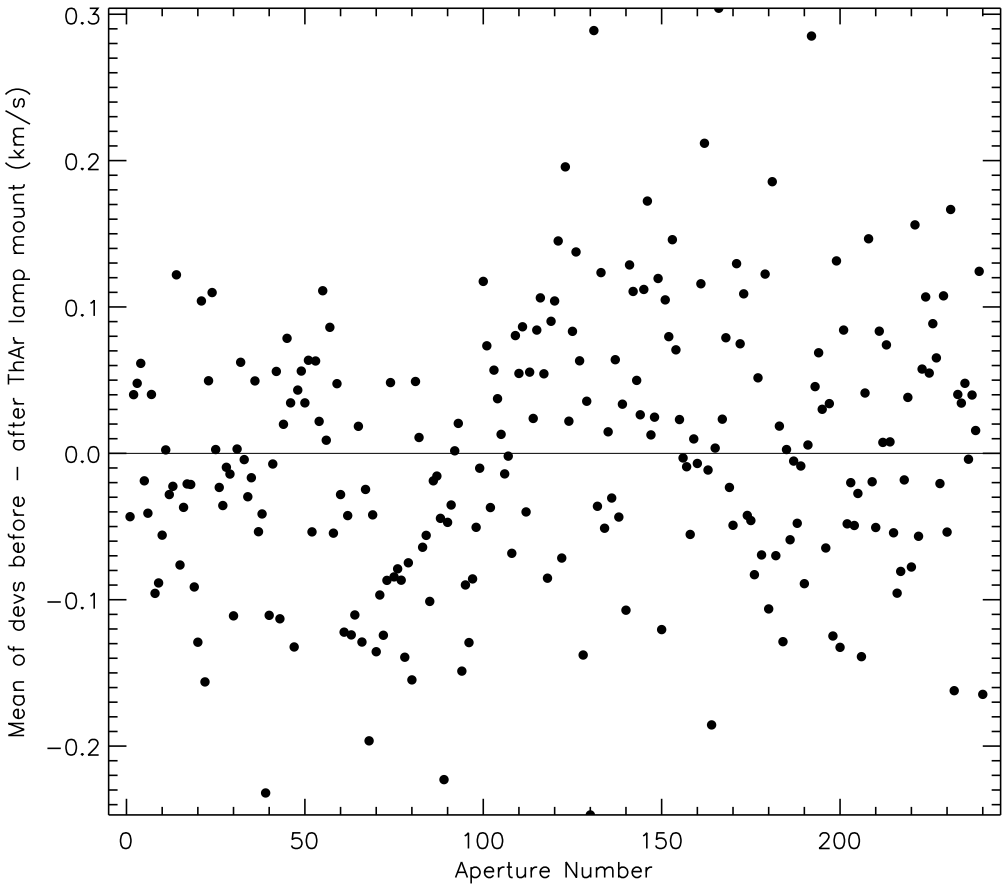

Figure A.13: The difference between the mean of the fall 2005 deviations and the mean of the spring 2006 deviations, for all 240 fibers.

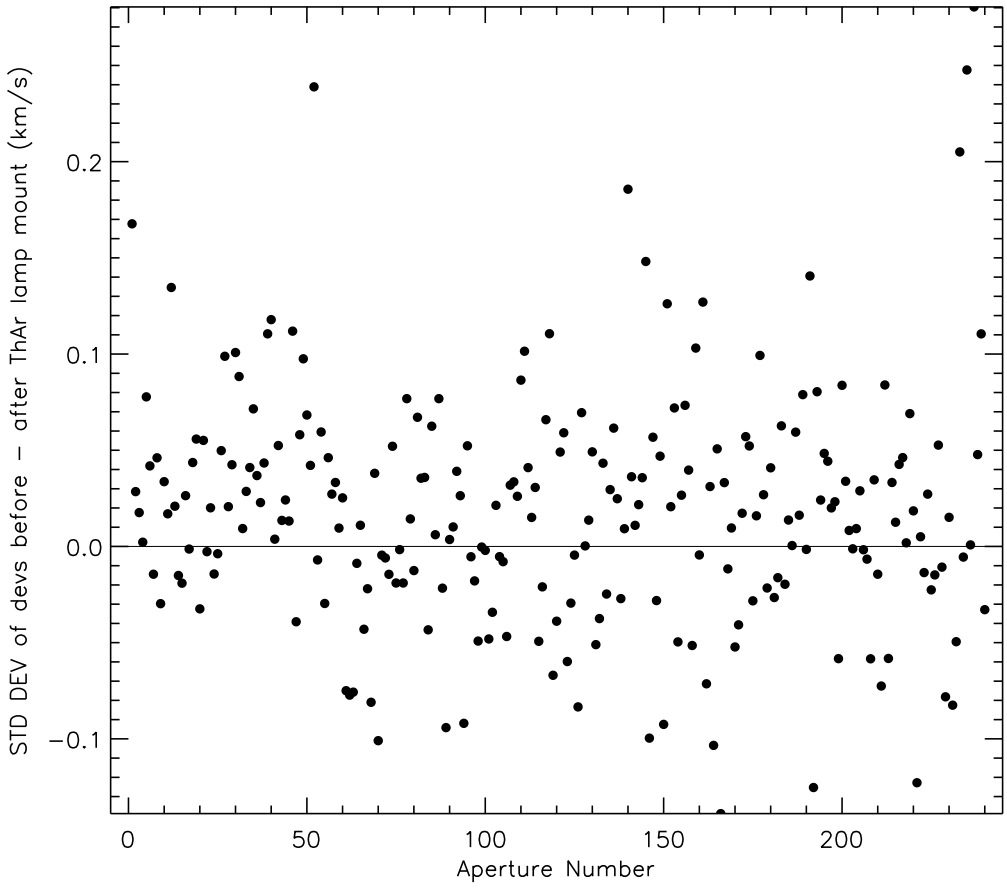

Figure A.14: The difference between the standard deviation of the fall 2005 deviations and the standard deviation of the spring 2006 deviations, for all 240 fibers.